Statistical theory of mixtures with surfactants

Wojciech T. Góźdź

January 1996

ACKNOWLEDGMENTS

I would like to express my gratitude to my adviser, doc. dr hab. Robert Hołyst, for his sincere interest in, and support of my work. I would like to express my special thanks to Professor Jan Stecki, whose influence on my professional life has been enormous, although indirect. My MSc thesis advisor, Professor Stefan Sokołowski, and my PhD advisor have done their PhD under supervision of Professor Stecki. It has been pleasure to me to work on my PhD thesis in the department, whose head is Professor Stecki. I have met there many people, with whom I enjoyed discussing, arguing, and socializing. I will remember for a long time discussions with: doc. dr hab. A. Ciach, dr. A. Maciołek, dr E. Naumowicz-Węglinska, dr hab. A. Poniewierski, dr A. Samborski, dr S. Wieczorek, dr A. Żywociński.

The calculations have been done on the computers sponsored by Fundacja Współpracy Polsko-Niemieckiej.

This work was supported by Komitet Badań Naukowych.

Contents

List of Figures

List of Tables

Chapter 1

Introduction: What is a microemulsion ?

Amphiphilic molecules are composed of two different parts: hydrophobic tail and hydrophilic head. An example of an amphiphilic molecule is shown in Fig. 1.1. The tail is composed of one or more hydrocarbon chains, usually with 6 to 20 carbon atoms, the head is composed of chemical groups of high affinity to water [1, 2]. Such a composition of amphiphilic molecules results in many amazing properties of systems containing these molecules. Adding an appropriate amount of amphiphile to a mixture of oil and water, two liquids which are immiscible under normal conditions, causes complete mixing of these liquids. The amount of amphiphile necessary to cause mixing depends on the strength of amphiphile. The longer the hydrocarbon chain the stronger the amphiphile is. The strength of amphiphile depends in similar way on the number of hydrophilic groups in the amphiphilic molecule. Complete mixing

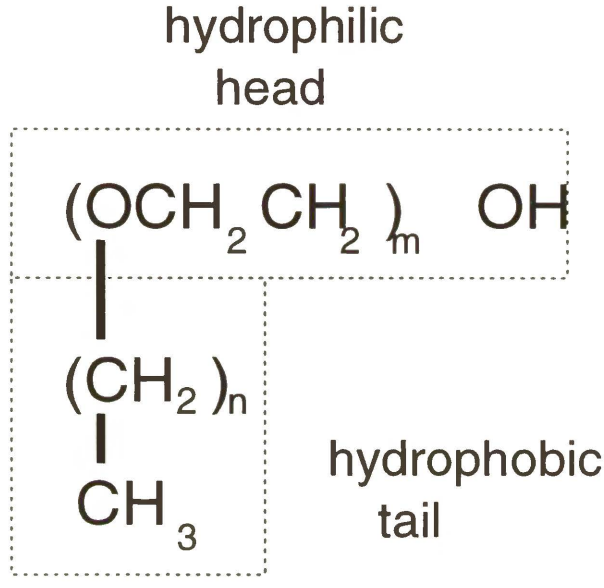

Figure 1.1: A non-ionic surfactant C_nE_m. Alkylpolyoxyethylen

is enabled by lowering the oil-water surface tension by amphiphile. That is why the amphiphilic molecules are also called surfactants: surface active agents. The surfactant assembles at the interface, forming a monolayer, in such a way that the hydrophilic part of the amphiphile is located in water and hydrophobic part in oil. The surfactant monolayer separates coherent regions of oil and water. Usually the monolayer width is small compared to the size of oil and water regions, unless the concentration of surfactant is very high. In such a situation the formation of water and oil droplets suspended in the surfactant solution is possible. Surfactants dissolved in water can form micells of different shape: spherical or cylindrical. They can also assemble into bilayers grouping the hydrophobic part of the surfactant

inside the bilayer. Such system is called the sponge phase.

When comparable amount of oil and water are mixed with surfactant a new homogeneous, isotropic, thermodynamically stable phase is created [3]. This phase, called microemulsion, can coexist with oil and water [4, 1, 2]. The measurements of electrical conductivity, self diffusion, NMR and freeze fracture microscopy studies indicate that the structure of microemulsion is bicontinuous [5, 6, 1, 7, 8]. That is the microemulsion is composed of water and oil channels mutually interwoven, separated by the monolayer of surfactant. The description of microemulsion structure is a challenge for modern condensed matter physics.

The amphiphilic systems can form apart from the structured disordered phase like microemulsion, many ordered phases. The most common are the lamellar and hexagonal. The lamellar phase is composed of the regions of water and oil separated by the surfactant monolayer. The lamellar phase looks like a sandwich composed of the slices of water and oil separated by a monolayer of surfactant. The hexagonal phase is composed of cylinders of water or oil bounded by the layer of surfactant, arranged on a hexagonal lattice, immersed in oil or water. The most interesting are the ordered cubic bicontinuous phases. The most prominent examples are the gyroid, double diamond (sometimes called diamond), and simple cubic phase. Although the structure of a bicontinuous phase on a mesoscopic scale is difficult to study experimentally, the experimental methods like freeze fracture microscopy or x-ray and neutron scattering revealed some details. In the scattering experiments one is able to study the symmetry, the freeze fracture microscopy gives

some information about the topology.

The systems containing surfactants are difficult to characterize. They are structured liquid ternary mixtures. For example microemulsion on a macroscopic level looks like an ordinary, homogeneous fluid. However, it is known that the microemulsion is composed of three components: two of them, oil and water do not mix in the absence of the third one, the surfactant. Thus the presence of the surfactant is crucial. It is obvious that information about the location of surfactant in its mixtures characterizes the mixtures in the best way. **The surfactant forms a monolayer at the water-oil interface. This monolayer can be approximated in the theory by a mathematical surface. Thus in order to characterize the systems containing surfactants it is enough to characterize this surface and its properties such as the surface area, genus and its curvatures** [9, 10, 11, 12, 13].

There are three levels of description of these mixtures: macroscopic, mesoscopic, and microscopic. Here we concentrate on the mesoscopic level, described by the Landau-Ginzburg theory developed recently. We note that the most interesting phenomena take place on the mesoscopic scale, that is intermediate between the microscopic and macroscopic. The typical sizes of oil-rich domains in the mixture are often of the size of 1000Å, a size much larger than the size of a surfactant (25Å), but much smaller than the macroscopic scale of millimeters [1]. **It means that microemulsion is structured on the mesoscopic scale and that fact justifies the choice of the Landau-Ginzburg model for its descriptions.** In the next section

we describe the Landau-Ginzburg theory that we use to generate the surfaces in the oil, water, surfactant mixtures.

Chapter 2

Landau-Ginzburg model

The theoretical model describing the behavior of the system containing surfactants originates form the expansion in gradients of the Landau-Ginzburg free energy [14]:

$$\begin{aligned}\mathcal{F}[\phi(\mathbf{r})] = \int d^3\mathbf{r}\Big(& a_0 + a_1\phi(\mathbf{r}) + a_2\phi(\mathbf{r})^2 + a_3\phi(\mathbf{r})^3 + a_4\phi(\mathbf{r})^4 \\ & + a_5\phi(\mathbf{r})^5 + a_6\phi(\mathbf{r})^6 + \cdots \\ & + c_1 \mid \nabla\phi(\mathbf{r}) \mid^2 + c_2 \mid \triangle\phi(\mathbf{r}) \mid^2 + \cdots \\ & + \phi(\mathbf{r})^2 \mid \nabla\phi(\mathbf{r}) \mid^2 + \cdots \Big).\end{aligned} \tag{2.1}$$

This is the simplest model with a single scalar order parameter $\phi(\mathbf{r})$. The analysis of (2.1) shows that the essential features of systems with internal interfaces can be recovered by keeping $c_1 < 0$ and $c_2 > 0$. The gradient term with negative coefficient c_1 tends to create the interface, whereas the laplacian term with the positive coefficient c_2 stabilizes the system. The

number of terms and the values of coefficients, in the expansion of the scalar order parameter $\phi(\mathbf{r})$ in power series, depends on the problem to be studied. In order to study microemulsion and ordered phases which appear in systems containing surfactants the following Landau-Ginzburg functional was proposed [15, 16] based on (2.1)

$$\mathcal{F}[\phi(\mathbf{r})] = \int d^3\mathbf{r}\Big(c \mid \triangle\phi(\mathbf{r}) \mid^2 + g[\phi(\mathbf{r})] \mid \nabla\phi(\mathbf{r}) \mid^2 + f[\phi(\mathbf{r})] + \mu\phi(\mathbf{r})\Big). \tag{2.2}$$

The values of the field $\phi(\mathbf{r})$ are proportional to the difference in oil and water concentrations and are negative for water and positive for oil region or vice versa. The sign is just the matter of convention. The surface

$$\phi(\mathbf{r}) = 0 \tag{2.3}$$

describes the interface between oil and water. The function $f[\phi(\mathbf{r})]$ is the bulk free energy. μ is the chemical potential difference between oil and water. The surfactant degrees of freedom are considered as being integrated out and the surfactant properties enter the functional (2.2) through the form of the functions $g[\phi(\mathbf{r})]$ and $f[\phi(\mathbf{r})]$. The functional (2.2) can be also used to model the sponge phase. In such a case the negative values of order parameter are interpreted as the interior part of the sponge phase and positive as exterior part of the phase (or vice versa).

The thermodynamic quantities and correlation functions can be obtained from (2.2) by functional integration. The two point correlation function is given by

$$< \phi(\mathbf{r_1})\phi(\mathbf{r_2}) >= \frac{\int D\{\phi(\mathbf{r})\}\phi(\mathbf{r_1})\phi(\mathbf{r_2})\exp\{-\mathcal{F}[\phi(\mathbf{r})]\}}{\int D\{\phi(\mathbf{r})\}\exp\{-\mathcal{F}[\phi(\mathbf{r})]\}}. \tag{2.4}$$

The functional integration cannot be usually performed exactly. One has to use some approximation method to evaluate the functional integral. The most often used is mean-field approximation, in which the integral is replaced with the maximum of the integrand, i.e. one has to find the minimum of $\mathcal{F}[\phi(\mathbf{r})]$, which satisfy the mean-field equation

$$\frac{\delta\mathcal{F}[\phi(\mathbf{r})]}{\delta\phi(\mathbf{r})} = 0. \tag{2.5}$$

In the Gaussian approximation the water-water structure factor $S_{ww}(k)$ (Fourier transform of the correlation function (2.4)) for (2.2) is given by

$$S_{ww}(k) \propto \frac{1}{ck^4 + g(\phi_b)k^2 + \frac{1}{2}f''(\phi_b)}, \tag{2.6}$$

$\phi_b \in \{\phi_w, \phi_m, \phi_o\}$, and for oil-rich phase $< \phi(\mathbf{r}) > \simeq \phi_o$, for water-rich phase $< \phi(\mathbf{r}) > \simeq \phi_w$, for microemulsion $< \phi(\mathbf{r}) > \simeq \phi_m = 0$. A peak at $k > 0$ (for $\phi_b = \phi_m$) indicates a local structure of microemulsion with characteristic size

$\xi \sim \frac{2\pi}{k}$. For $\phi_b = \phi_o$ or ϕ_w the structure factor has a peak only at $k = 0$ indicating that pure oil and water phase behaves like normal liquid with no internal structure. The water-water structure factor $S_{ww}(k)$ can be measured in experiments. Thus the quality of the theory can be checked out by comparing theoretical predictions with an experiment. It turns out that (2.6) describes extremally well the data from the scattering experiments [15, 7]. The model (2.2) has been successfully used to describe wetting behavior of the microemulsion at the oil-water interface [16, 17, 18, 19], to investigate a few ordered phases such as lamellar, double diamond, simple cubic, hexagonal or crystals of spherical micells [20, 21], and to study the mixtures cotaining surfactant in confined geometry [22] .

An enormous advantage of the model (2.2) is its simplicity. It is extraordinary that the properties of a very complex system are described by the one scalar order parameter field. There are a few Landau-Ginzburg theories with more than one order parameter field [5, 23, 24, 25, 26, 27]. However, adding a new order parameter field does not automatically make the model better. It does, for sure, make solving the model more difficult and it involves introduction of new parameters, physical meaning of which is not always clear.

We have used in our calculations the model (2.2) with the functions $g[\phi(\mathbf{r})]$, $f[\phi(\mathbf{r})]$ given by

$$g\big[\phi(\mathbf{r})\big] = g_2\phi(\mathbf{r})^2 + g_0, \tag{2.7}$$

$$f\big[\phi(\mathbf{r})\big] = \omega\Big(\phi(\mathbf{r}) + \phi_w\Big)^2\Big(\phi(\mathbf{r})^2 + f_0\Big)\Big(\phi(\mathbf{r}) + \phi_o\Big)^2 \tag{2.8}$$

and following set of constants: $\phi_o = -\phi_w = 1$, $c = 1$, $\omega = 1$, $\mu = 0$. Thus the functional (2.2) takes the form

$$\mathcal{F}[\phi(\mathbf{r})] = \int d^3\mathbf{r}\Big(\mid \triangle\phi(\mathbf{r}) \mid^2 + (g_2\phi(\mathbf{r})^2 + g_0) \mid \nabla\phi(\mathbf{r}) \mid^2 + (\phi(\mathbf{r})^2 - 1)^2(\phi(\mathbf{r})^2 + f_0)\Big). \tag{2.9}$$

The function $f[\phi(\mathbf{r})]$ has by construction three minima, which guarantees three phase coexistence, i.e. oil, water, and microemulsion. The minima for oil-rich and water-rich phase are of equal depth, which makes the system symmetric, therefore μ has to be set to zero. Varying the parameter f_0 makes the middle phase (microemulsion) more or less stable with respect to two bulk phases. Thus f_0 is proportional to the chemical potential of microemulsion. The constant g_2 depends on g_0 and f_0 and is chosen in such a way that the correlation function $G(r) =< \phi(\mathbf{r})\phi(\mathbf{0}) >$ decays monotonically in the oil-rich and water-rich phases. Here we take $g_2 = 4\sqrt{1 + f_0} - g_0 + 0.01$. The more negative g_0 the stronger or the more surfactant is used.

In the mean-field approximation the stable or metastable phases of the system correspond to the minimum of the functional (2.2). Finding the minima of the functional (2.2) is not a trivial task. There are not known analytic methods to deal with such problems. In the case of bicontinuous phases two methods have been used with some success. The first is expansion of the order parameter in a Fourier series, the second is Monte Carlo simulation.

The Fourier series approach was used by Gompper and Zschocke [21]. They expanded the order parameter $\phi(\mathbf{r})$ in the following way:

$$\phi(\mathbf{r}) = \sum_{i=0}^{N} \sum_{\mathbf{K} \in B_i} \phi_{\mathbf{K}} \cos(\mathbf{K} \cdot \mathbf{r}), \tag{2.10}$$

where sum runs over all reciprocal lattice vectors of a given lattice structure, B_i denotes the ith shell of the reciprocal lattice. Such approach has a few disadvantages. One has to know a priori how the solution looks like to be able to construct the Fourier series. The quality of the Fourier expansion is not know, because it is difficult to say in advance how many shells have to be taken to approximate well the investigated structures. Moreover the number of shells taken in the approximation is limited, because the more shells are taken the more variables have to be minimized.

The Monte Carlo method, used by Gompper and Kraus [28] seems to be an ideal solutions. However, it also has some disadvantages. The continuous model has to be discretized. The quality of discretization depends on the size of the lattice which is limited by the speed of computers and the computer memory. Due to the fluctuations, taken into account in simulations, the local properties of the functional, as e.g. the shape of the interface given by $\phi(\mathbf{r}) = 0$, cannot be described with sufficient accuracy.

The method we propose is a new one. It requires the discretization of a continuous model as in the Monte Carlo simulations, but the local properties of the structures can be computed with very high accuracy. Moreover the

topology of the investigated structures does not have to be known in advance. This is enormous advantage of the method, as our results show it would be very hard to imagine the topology of many structures discovered by us.

As we have noticed in the Introduction the crucial information about the structure are contained in the properties of the surface $\phi(\mathbf{r}) = 0$ formed, in the system, by surfactant. We have observed [29] the very special property of the functional (2.9) related to this surface. We have discovered it by analyzing the formula for the mean curvature expressed in terms of the three dimensional field $\phi(\mathbf{r})$. From the form of (2.9) one can realize that indeed for some local minima of (2.9) the average curvature given by

$$H(\mathbf{r}) = -\frac{1}{2}\nabla\left(\frac{\nabla\phi(\mathbf{r})}{|\nabla\phi(\mathbf{r})|}\right) = -\frac{1}{2}\frac{\triangle\phi(\mathbf{r})}{|\nabla\phi(\mathbf{r})|} + \frac{\nabla\phi(\mathbf{r})\nabla|\nabla\phi(\mathbf{r})|}{2|\nabla\phi(\mathbf{r})|^2} \tag{2.11}$$

vanishes at every point of the $\phi(\mathbf{r}) = 0$ surface. It follows from the second term of (2.9) that $|\nabla\phi(\mathbf{r})|$ should have the maximal value for $\phi(\mathbf{r}) = 0$ (note that $g_0 < 0$) and consequently the second term (which after a small algebra can be written as $(\partial|\nabla\phi(\mathbf{r})|/\partial n)/2|\nabla\phi(\mathbf{r})|$, with ∂n denoting the derivative along the normal to the surface) in (2.11) vanishes. Also for the $\phi(\mathbf{r})$, $-\phi(\mathbf{r})$ symmetry we know that $H(\mathbf{r})$ averaged over the whole surface should be zero. It means that either $\triangle\phi(\mathbf{r})$ is exactly zero at the surface or it changes sign. From the first term of (2.9) it follows that the former is favored and consequently $H(\mathbf{r}) = 0$ at every point $\mathbf{r}$ at the surface $\phi(\mathbf{r}) = 0$. The surface such that the mean curvature vanishes at its every point is called minimal, Fig. 2.1 . Therefore before solving (2.9) we observe that among the local

minima of the functional (2.9) the structures with minimal surfaces should be favored.

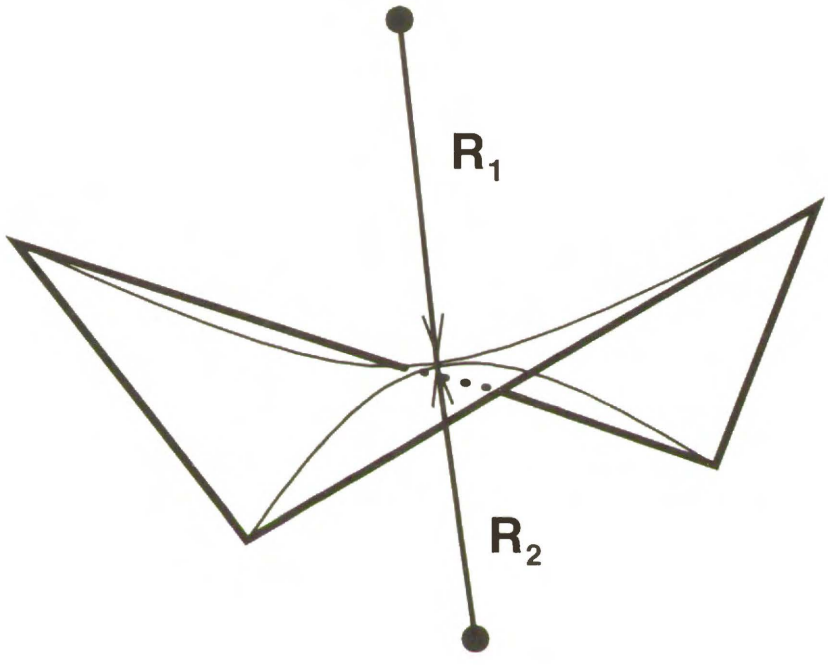

Figure 2.1: The figure illustrates a piece of surface with non-positive Gaussian curvature. R_1 and R_2 are the principal radii. The Gaussian (K) and the mean (H) curvatures are expressed in terms of the principal radii as follows: $H = \frac{1}{2R_1} + \frac{1}{2R_2}$, $K = \frac{1}{R_1 R_2}$. If $R_1 = -R_2$, at every point, the surface is called minimal. This implies that K is non-positive at every point.

Chapter 3

Minimization of the functional

In order to find the local minima of the functional (2.9) we have discretized it on the cubic lattice. Thus the functional $\mathcal{F}[\phi(\mathbf{r})]$ becomes a function $F(\{\phi_{i,j,k}\})$ of N^3 variables, where $L = (N-1)h$ is the linear dimension of the cubic lattice, h is the lattice spacing, and $\{\phi_{i,j,k}\}$ stands for the set of all variables of the function. Each variable $\phi_{i,j,k}$ represents the value of the field $\phi(\mathbf{r})$ at the point $\mathbf{r} = (i,j,k)h$, and $i,j,k = 1,\ldots,N$. In our calculations we use N=129, which results in over 2 million points per unit cell.

3.1 Periodic Boundary Conditions

All structures we have investigated are periodic. Thus periodicity had to be incorporated into the functional (2.9). It was done by periodic boundary conditions:

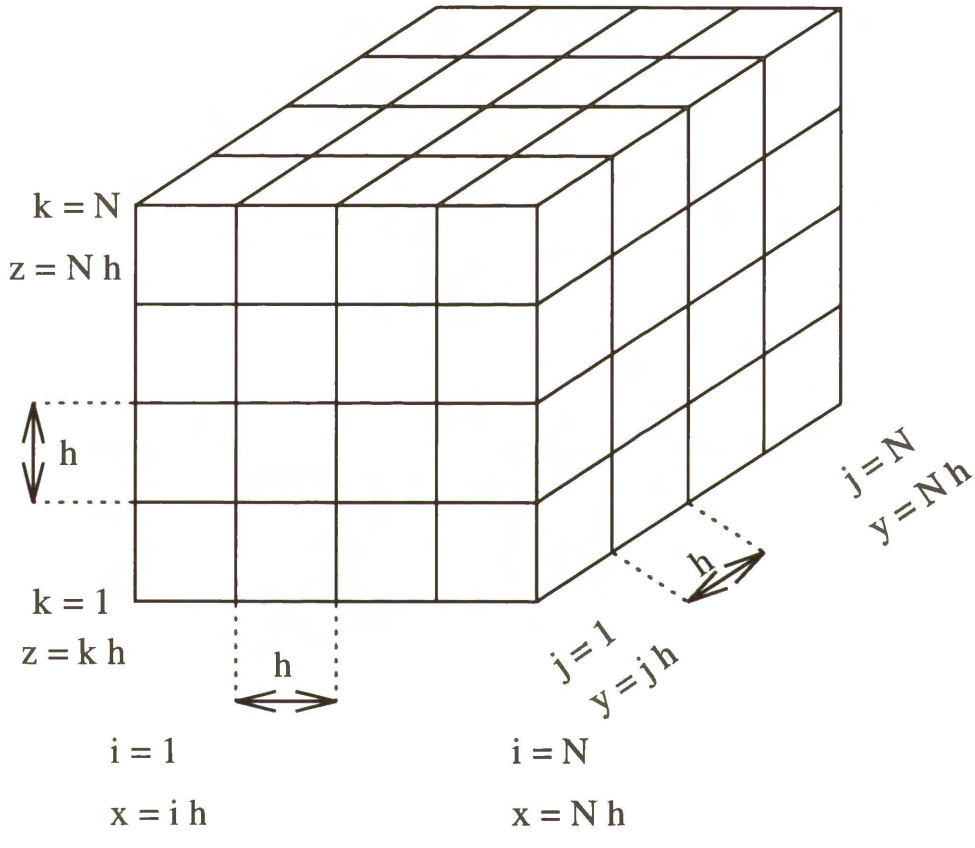

Figure 3.1: The schematic illustration of the cubic lattice used to discretize the functional (2.2). The number of lattice sites is N^3, the lattice spacing is h. The linear dimension of the lattice is $L = (N-1)h$.

$$\phi_{1,j,k} = \phi_{N,j,k} \tag{3.1}$$

$$\phi_{2,j,k} = \phi_{N+1,j,k}, \qquad \phi_{3,j,k} = \phi_{N+2,j,k} \tag{3.2}$$

$$\phi_{0,j,k} = \phi_{N-1,j,k}, \qquad \phi_{-1,j,k} = \phi_{N-2,j,k} \tag{3.3}$$

and similar in y and z directions. The points outside the unit cell, given by the periodic boundary conditions, enter the functional through the calculations of derivatives of points at the boundary and near the boundary of the lattice, i.e. when at least one of the indices i, j, k is equal to $1, 2, N-1, N$.

3.2 Discretization of derivatives

The first and second derivatives in the gradient and laplasian term of the functional (2.9) at the point $\mathbf{r} = (i, j, k)h$ on the lattice were calculated according to the following formulas [30]

$$\frac{\partial \phi(\mathbf{r})}{\partial x} \to \frac{\phi_{i+1,j,k} - \phi_{i-1,j,k}}{2h}, \tag{3.4}$$

and

$$\frac{\partial^2 \phi(\mathbf{r})}{\partial x^2} \to \frac{1}{12h^2}\Big(-\phi_{i+2,j,k} + 16\phi_{i+1,j,k} - 30\phi_{i,j,k} + 16\phi_{i-1,j,k} - \phi_{i-2,j,k}\Big), \tag{3.5}$$

and similar in y and z directions.

The mixed derivatives used in (3.15), (3.16) are calculated according to [30]

$$\frac{\partial^2\phi(\mathbf{r})}{\partial x\partial y} \to -\frac{1}{2h^2}\Big(\phi_{i+1,j,k}+\phi_{i-1,j,k}+\phi_{i,j+1,k}+\phi_{i,j-1,k} - 2\phi_{i,j,k}-\phi_{i+1,j+1,k}-\phi_{i-1,j-1,k}\Big). \tag{3.6}$$

Fig. 3.2 illustrates calculation of derivatives on the cubic lattice of: (a) first derivatives given by (3.4) , (b) second derivatives given by (3.5) , (c) mixed derivatives given by (3.6). In our calculations we used 5-point formula (3.5) to calculate the second derivatives in laplasian term in order to have more accurate approximation for small lattice size. However the 3-point formula given by [30]

$$\frac{\partial^2\phi(\mathbf{r})}{\partial x^2} \to \frac{1}{h^2}(\phi_{i+1,j,k}-2\phi_{ijk}+\phi_{i-1,j,k}) \tag{3.7}$$

can also be used. We have compared the values for the free energy density calculated for 3-point and 5-point approximation of the second derivatives. It turned out that the values of the free energy density differed for small lattice size, $N = 9$, but for big lattice size, $N = 129$, the difference was negligible and both approximations are equally good. Moreover, the calculation of derivatives on the lattice boundary requires taking into account the points outside the lattice. These points are given by periodic boundary conditions, because we have studied periodic structures. Thus the periodicity is better

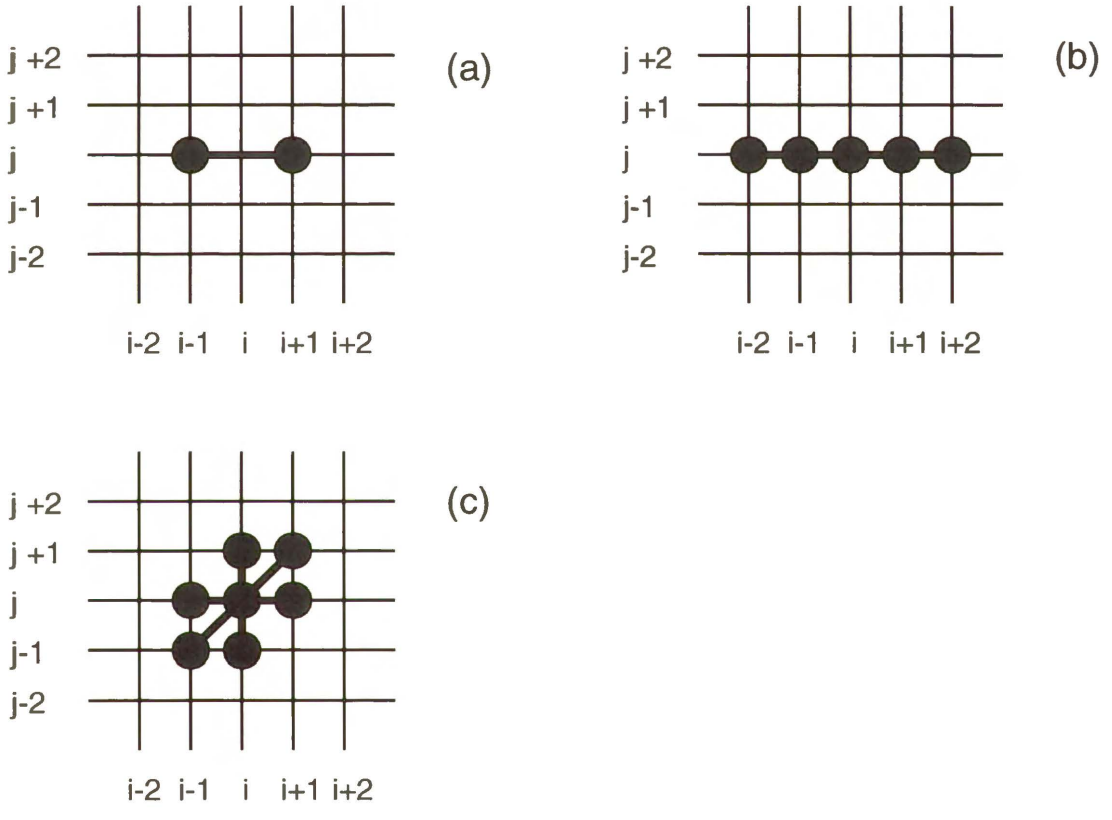

Figure 3.2: The schematic illustration of formulas used to calculate the derivatives of the discretized functional: (a) formula (3.4), (b) formula (3.5), (c) formula (3.6). The black circles show the points taken in calculation of the derivatives.

incorporated into the discretized functional by the 5-point formula, because it uses more points outside the unit cell.

3.3 Choosing the surface

The order parameter field $\phi(\mathbf{r})$ carries enormous amount of information about the local structure of the phases we have investigated. The most interesting is the topology of the phases, described by the surface

$$\phi(\mathbf{r} = (x, y, z)) = 0, \tag{3.8}$$

dividing positive and negative regions of the order parameter field. Thus it was crucial in our studies to find the location of the surface $\phi(\mathbf{r}) = 0$.

It is highly unlikely, because of numerical accuracy, that a value of the field $\phi(\mathbf{r}) = \phi_{i,j,k}$ at the point $\mathbf{r} = (i, j, k)h$ on the lattice is exactly zero. Therefore the points of the surface have to be localized by interpolation between the neighboring sites of the lattice. If $\phi(\mathbf{r}_1 = (i, j, k)h) = \phi_{i,j,k} < 0$ and $\phi(\mathbf{r}_2 = (i+1, j, k)h) = \phi_{i+1,j,k} > 0$ then the point $\mathbf{r}_0$, for which $\phi(\mathbf{r}_0) = 0$, must lie between the points $\mathbf{r}_1 = (i, j, k)h$ and $\mathbf{r}_2 = (i + 1, j, k)h$. Moreover, the location of $\mathbf{r}_0$ depends on the values of the field at the points $\mathbf{r}_1$ and $\mathbf{r}_2$ in the following way

$$\mathbf{r}_0 = \left(i + \frac{|\phi_{i,j,k}|}{|\phi_{i,j,k} - \phi_{i+1,j,k}|}, j, k \right) h. \tag{3.9}$$

This approximation is legible because the field $\phi(\mathbf{r})$ is very smooth. Fig. 3.3

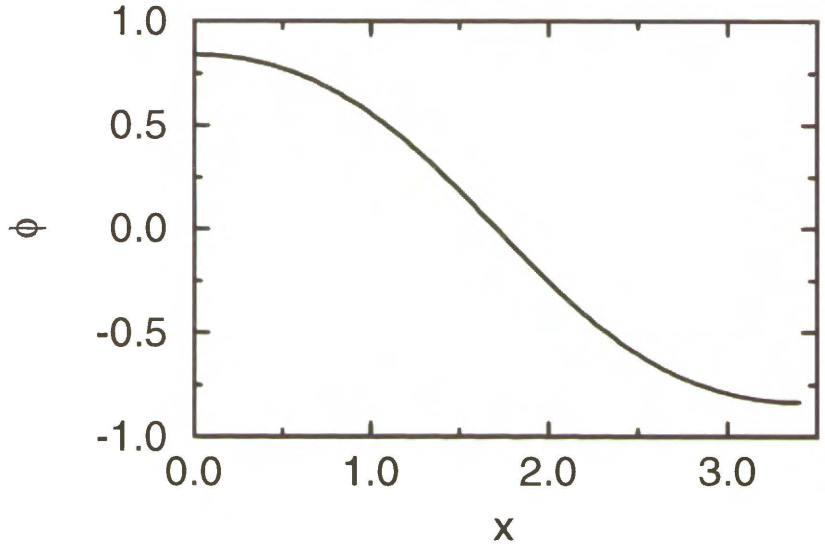

Figure 3.3: The order parameter profile $\phi(x)$ for the lamellar phase, calculated from the functional (2.9) for the parameters $f_0 = 0$ and $g_0 = 0$. Half of the unit cell is presented. Here $N = 400$, thus, h, the distance between the lattice size is $3.4/400 = 0.0085$. Certainly this justifies the linear interpolation.

shows the profile of the order parameter $\phi(x)$ for the lamellar phase. In the vicinity of $\phi(x) = 0$ the profile is almost a straight line. Thus for small values of lattice spacing, h, finding the points of the surface $\phi(\mathbf{r}) = 0$ should not introduce significant errors. As our calculations show it is done with high accuracy.

3.4 Triangulation, Surface Area, Volume

In the way described in the preceding section one can find the points of the surface $\phi(\mathbf{r}) = 0$ located between the neighboring lattice sites. However this is not enough to describe the surface. It is also necessary to specify the connections between these points to characterize the surface.

Due to discretization the unit cell is divided on $(N-1)^3$ small cubes of the size of lattice spacing, h. The surface $\phi(\mathbf{r}) = 0$ passing through a small cube cuts out of it a polygon, which edges are formed by intersection of the surface and faces of the small cube. The edges of the polygon can be approximated by straight lines. The possible configurations of the surface $\phi(\mathbf{r}) = 0$ cutting a small cube are pictured in Fig. 3.4. The surface $\phi(\mathbf{r}) = 0$ can cut out only four kinds of polygons: a triangle, a tetragon, a pentagon, a hexagon. The edges of these polygons except a triangle do not lie in a common plane. It is necessary to specify also the connections between the vertices of the polygon, to characterize the surface unambiguously. It was done in the way shown in Fig. 3.4 with thick dotted lines in the patches of the surface inside the small cubes. This procedure makes the surface covered only with triangles. The triangulation described above was used to calculate the surface area inside a unit cell by summing up the surface area of all triangles.

The triangulation was also used to calculate the volume ratio of the two subvolumes.The surface $\phi(\mathbf{r}) = 0$ separates the volume of a given phase into two subvolumes, first occupied by the field $\phi(\mathbf{r}) > 0$ and second by $\phi(\mathbf{r}) < 0$. In order to calculate the volume occupied by the negative or

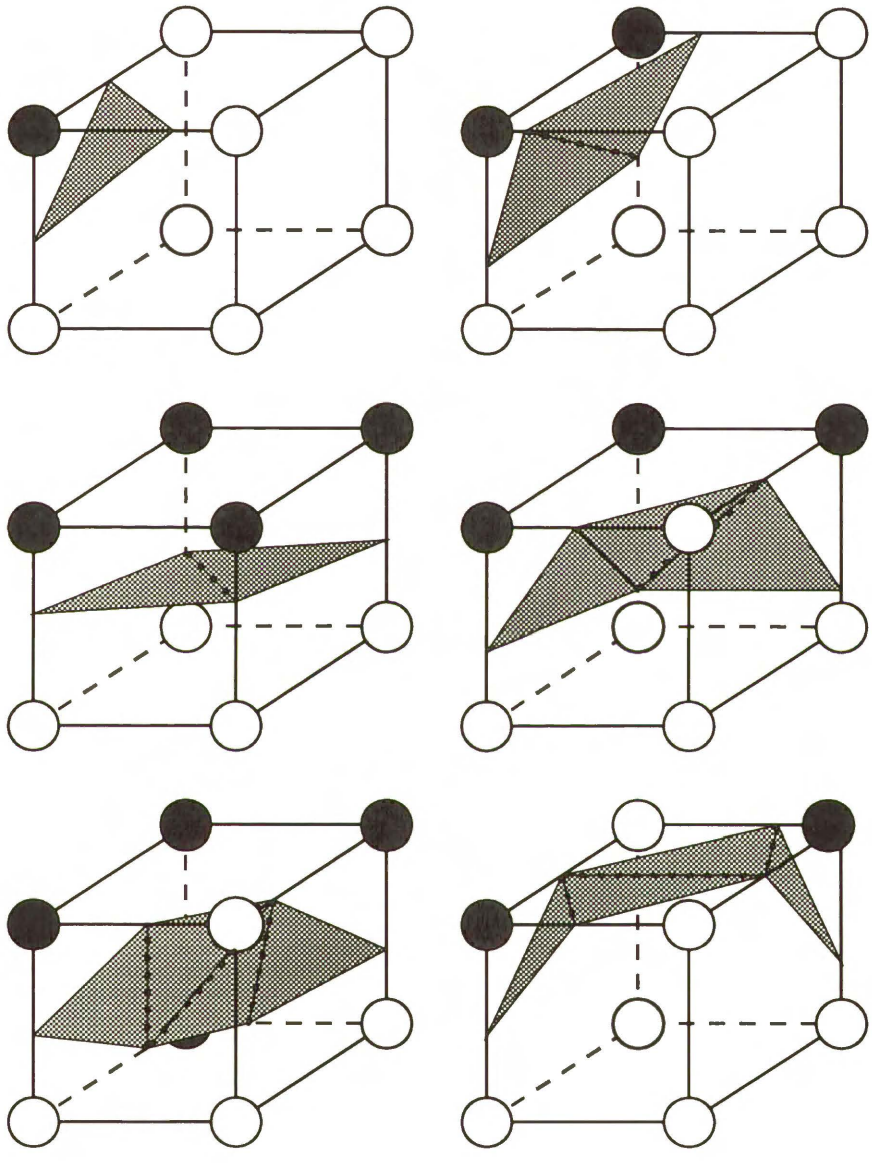

Figure 3.4: The possible configurations of passing the surface $\phi(\mathbf{r}) = 0$ through the field $\phi(\mathbf{r})$ discretized on the lattice. Black circles represent $\phi_{i,j,k} < 0$, whereas white circles $\phi_{i,j,k} > 0$. The cubes represent the smallest pieces, of the lattice of the linear dimension, h.

positive values of the field $\phi(\mathbf{r})$ the volume of the small cubes not cut by the surface $\phi(\mathbf{r}) = 0$ is calculated. Next we use the triangulated surface $\phi(\mathbf{r}) = 0$ to divide the small cubes with the values of the field $\phi(\mathbf{r})$ of different sign at the vertices. The surface $\phi(\mathbf{r}) = 0$ divides a small cubes into two polyhedra. The volumes of these polyhedra for negative and positive values of the field $\phi(\mathbf{r})$ was calculated and added to the previously calculated volume for regions of positive and negative values of $\phi(\mathbf{r})$.

For more than one periodic surface, in the unit cell, it is necessary to separate different surfaces to be able to calculate surface area and genus of each surface. In order to find the points which belong to the same surface one has to chose an arbitrary point on one of the surfaces and following the connections between points find the rest of the points belonging to this surface. The set of connections will uniquely specify the surface. Fig. 3.5 illustrates the way this process can be done for two surfaces. Having chosen an arbitrary point on one surface, represented by a black circle in Fig. 3.5a, one has to find among all the connections between couples of points specified by the triangulation, the connections including this point. They are represented by thick solid lines connecting the black circle with the white circles. Next one has to chose arbitrarily a point among the points represented by white circles and find all connections between this point and the points remaining after removing from the set of connections the connections containing the first point. This is shown in Fig 3.5b. Such procedure has to be repeated until no more than one point represented by the white circle is left.

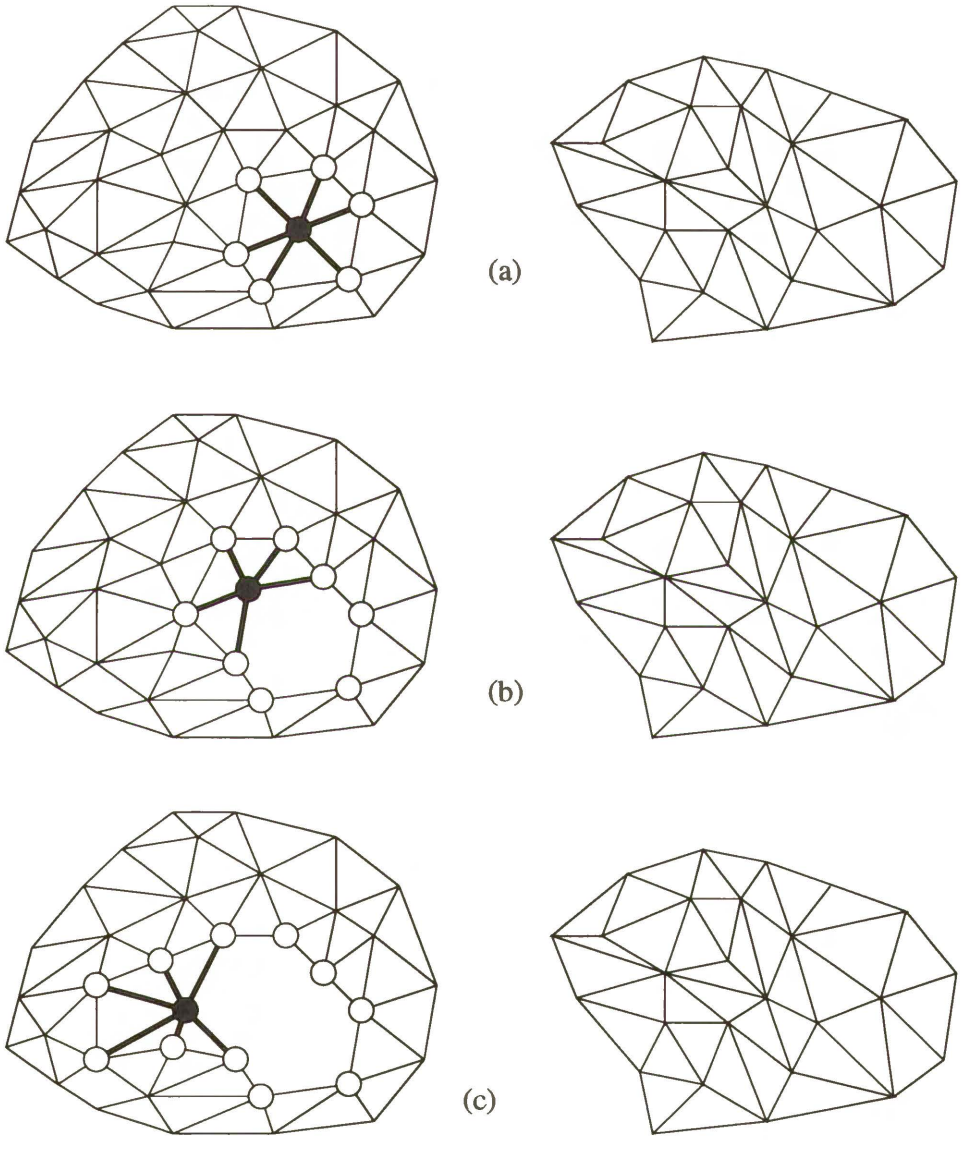

Figure 3.5: The schematic illustration of the separation of two disjoint surfaces.

3.5 Euler characteristics, genus

The triangulation can also be used to calculate the Euler characteristics, χ, of the surface inside the unit cell. The calculation of χ can be done according to the Euler formula [31]

$$\chi = F + V - E, \tag{3.10}$$

where F,V,E is the number of faces (F), vertices (V), and edges (E) of the polygons cut out by the surface $\phi(\mathbf{r}) = 0$ in the small cubes of dimension of lattice spacing, (Fig. 3.5). The fact that each polygon is inside a small cube makes the calculation very easy, because each vertex of the polygon belongs to four polygons since it lies in the edge of the small cube. Therefore to calculate χ one does not need to know the connections between points. It is sufficient to know only how many times the surface $\phi(\mathbf{r}) = 0$ cuts the edges of the small cube and how many cubes it cuts. The number of faces (F) is therefore the number of small cubes cut by the surface $\phi(\mathbf{r}) = 0$, that is the cubes with the values of the field $\phi(\mathbf{r}) = \phi_{i,j,k}$ of different sign at its vertices. The number of vertices is given by the number of intersections of the surface $\phi(\mathbf{r}) = 0$ with the edges of the small cubs taken with a weight 1/4, because each edge belongs to four cubes. The number of edges (E) is the same as the number of vertices, but it has to be taken with a weight 1/2 because the polygon edges lie in the faces of small cubes and each face belongs to two cubes.

The Euler characteristic for the closed surface is related to the Gaussian (K) curvature and genus (g) of this surface in the following way [31, 32]

$$\chi = \frac{1}{2\pi}\int_S K dS = 2(1-g), \tag{3.11}$$

where the integral is taken over the surface S. Genus is an integer number and tells how many holes are in a closed surface. For example the genus for a sphere is zero, for a torus is one and for a pretzel is two. The structures we have investigated are infinite and periodic. The genus for an infinite surfaces is infinite, of course, but for a finite piece of this surface, in a unite cell, is finite and characterize the surface. Due to periodicity the unit cubic cell can be treated as a closed surface in four dimensions making calculation of genus for the infinite periodic surface fully justified [33]. Therefore the genera of the structures were calculated according to: $g = 1 - \chi/2$, where χ was the Euler characteristics for the surface inside a unit cell.

3.6 Curvatures

The Gaussian and the mean curvatures present another characteristics of the internal surfaces given by $\phi(\mathbf{r}) = 0$. In the description of the model we have mentioned that some of the structures in the model should be characterized by zero mean curvature at every point of the internal interface. Here we present the method used to compute Gaussian and mean curvatures. The unit normal $\mathbf{n}(\mathbf{r})$ at the point $\mathbf{r}$ is given by the gradient of the field $\phi(\mathbf{r})$:

$$\mathbf{n}(\mathbf{r}) = \frac{\nabla\phi(\mathbf{r})}{\mid \nabla\phi(\mathbf{r}) \mid}. \tag{3.12}$$

The mean (H) curvatures is given by the divergence of the unit vector [34], normal to the surface at the point $\mathbf{r}$, $\mathbf{n}(\mathbf{r})$

$$H(\mathbf{r}) = -\frac{1}{2}\nabla\mathbf{n}(\mathbf{r}) = -\frac{1}{2}\nabla\frac{\nabla\phi(\mathbf{r})}{\mid \nabla\phi(\mathbf{r}) \mid}. \tag{3.13}$$

and the Gaussian curvature (K) by the formula [35]

$$K(\mathbf{r}) = \frac{1}{2}(-(\partial_i n_j)^2 + (\nabla\mathbf{n}(\mathbf{r}))^2). \tag{3.14}$$

In numerical calculations of the curvatures we used the following formulas [34, 36]:

$$H = -\frac{1}{2\sqrt{\phi_x^2 + \phi_y^2 + \phi_z^2}}\frac{B}{A} \tag{3.15}$$

$$K = \frac{1}{\phi_x^2 + \phi_y^2 + \phi_z^2}\frac{C}{A} \tag{3.16}$$

where A, B , and C are obtained from:

$$det \begin{pmatrix} (\phi_{xx} - \lambda) & \phi_{xy} & \phi_{xz} & \phi_x \\ \phi_{yx} & (\phi_{yy} - \lambda) & \phi_{yz} & \phi_y \\ \phi_{zx} & \phi_{zy} & (\phi_{zz} - \lambda) & \phi_z \\ \phi_x & \phi_y & \phi_z & 0 \end{pmatrix} = A\lambda^2 + B\lambda + C \tag{3.17}$$

and are given by:

$$A = -\left(\phi_x^2 + \phi_y^2 + \phi_z^2\right) \tag{3.18}$$

$$\begin{aligned} B = \phi_x^2\left(\phi_{yy} + \phi_{zz}\right) + \phi_y^2\left(\phi_{xx} + \phi_{zz}\right) + \phi_z^2\left(\phi_{xx} + \phi_{yy}\right) \\ - 2\phi_x\phi_y\phi_{xy} - 2\phi_x\phi_z\phi_{xz} - -2\phi_y\phi_z\phi_{yz} \end{aligned} \tag{3.19}$$

$$\begin{aligned} C = &\phi_x^2(\phi_{yz}^2 - \phi_{yy}\phi_{zz}) + \phi_y^2(\phi_{xz}^2 - \phi_{xx}\phi_{zz}) + \phi_z^2(\phi_{xy}^2 - \phi_{xx}\phi_{yy}) \\ &+ 2\phi_x\phi_z(\phi_{xz}\phi_{yy} - \phi_{xy}\phi_{yz}) + 2\phi_x\phi_y(\phi_{xy}\phi_{zz} - \phi_{xz}\phi_{yz}) \\ &+ 2\phi_y\phi_z(\phi_{yz}\phi_{xx} - \phi_{xy}\phi_{xz}) \end{aligned} \tag{3.20}$$

The mean and Gaussian curvatures have to be computed at the points of the surface $\phi(\mathbf{r}) = 0$. These points do not lie exactly at the lattice sites. In order to calculate the derivatives of the field $\phi(\mathbf{r})$ at the point $\mathbf{r}_0$, for which $\phi(\mathbf{r_0}) = 0$, according to the formulas (3.4), (3.5), (3.6) the values of the field $\phi(\mathbf{r})$ at the points $\mathbf{r}_0 + (0, 0, h)$, $\mathbf{r}_0 + (0, h, 0)$, $\mathbf{r}_0 + (h, 0, 0)$, $\mathbf{r}_0 + (0, 0, 2h)$,

$\mathbf{r}_0 + (0, 2h, 0)$, $\mathbf{r}_0 + (2h, 0, 0)$, $\mathbf{r}_0 + (0, h, h)$, $\mathbf{r}_0 + (h, h, 0)$, $\mathbf{r}_0 + (h, 0, h)$ have to be interpolated. The way the interpolation is done is shown in Fig. 3.6. The

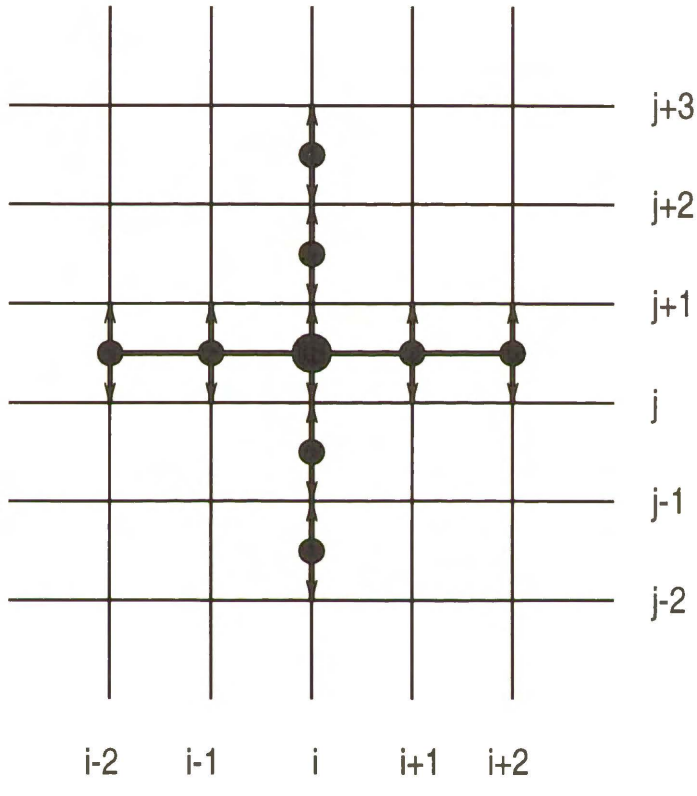

Figure 3.6: The way of interpolation of derivatives of the field $\phi(\mathbf{r})$ at the surface $\phi(\mathbf{r}) = 0$. The big black circle represents the point on the surface $\phi(\mathbf{r}) = 0$, the smaller black circles represent the points taken in calculations of derivatives. The arrows show the points on the lattice taken to interpolate the points between the lattice sites.

big black circle represents the point $\mathbf{r_0}$. The smaller black circles represent the points taken to calculate the derivatives. The values of the field in these points are interpolated from the values of the field at the nearest sites of the

lattice indicated by the arrows. The point $\mathbf{r_0}$ is $\frac{|\phi_{i,j,k}|}{|\phi_{i,j,k}-\phi_{i,j+1,k}|} = \Delta h$ away from the point $\mathbf{r} = (i,j,k)h$. Then the value of the field $\phi(\mathbf{r})$ at e.g. the point $\mathbf{r}_0 + (0,h,0)$ is $\Delta h(\phi_{i,j+1,k} - \phi_{i,j,k})$. The values of the field $\phi(\mathbf{r})$ in the remaining points can be calculated in a similar way.

It is remarkable that the properties characterizing two dimensional surface can be inferred from the three dimensional field.

3.7 Building initial configuration

The minimization procedure always requires an initial configuration. Here we present the initial configurations used in minimization of structures of different symmetries.

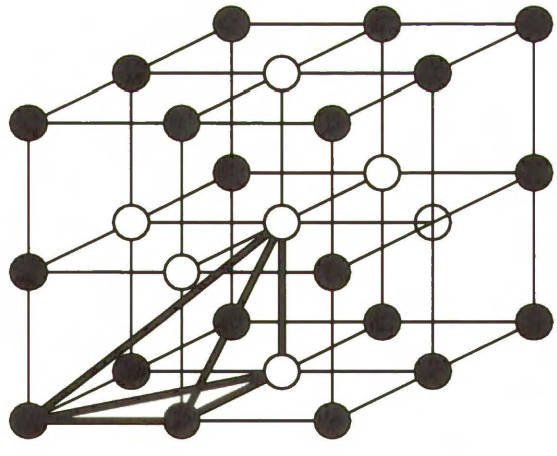

Figure 3.7: The initial configuration used to create structures of symmetry of simple cubic phase

The initial configuration is set up by building the field $\phi(\mathbf{r})$ for a unit cell

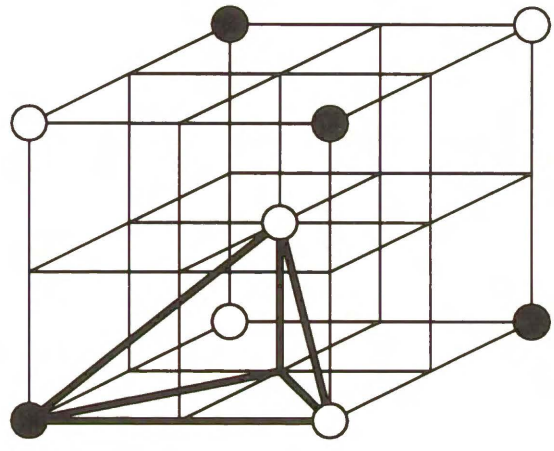

Figure 3.8: The initial configuration used to create structures of symmetry of double diamond phase

first on a small cubic lattice, $N = 3$ or 5, analogically to a two component, AB, molecular crystal. The value of the field $\phi(\mathbf{r}) = \phi_{i,j,k}$ at the point $\mathbf{r} = (i, j, k)h$ on the lattice is set to 1 if in the molecular crystal an atom A is in this place, if there is an atom B $\phi_{i,j,k}$ is set to -1, if there is an empty place $\phi_{i,j,k}$ is set to 0. Fig. 3.7 shows the initial configuration used to build the field $\phi(\mathbf{r})$ for the simple cubic phase unit cell. Filled black circles represent atoms of type A and hollow circles represent atoms of type B. In this case all sites are occupied by atoms A or B. Fig. 3.8 shows the initial configuration used to build the field $\phi(\mathbf{r})$ for the double diamond phase in 1/8 of the unit cell. There are unoccupied sites in this case and in these sites the value of the field $\phi(\mathbf{r}) = \phi_{i,j,k}$ is set to zero. It would be difficult to present the initial configuration for the gyroid phase, because it would require drawing the picture of lattice of size $N = 9$. Such a picture would be unreadable.

Therefore we present this configuration schematically in Fig. 3.9. The solid and dotted lines show the channels of oil and water. The thick dashed lines show the region occupied by rectangular parallelopiped used to build the unit cell. The fractions represent the value of z coordinate of an atom in the unit cell. In order to better visualize this configuration we present in Fig. 3.10 the points on the lattice, in a unit cell, with the values of the field $\phi(\mathbf{r})$ set initially to -1 (light grey spheres) and +1 (dark grey spheres).

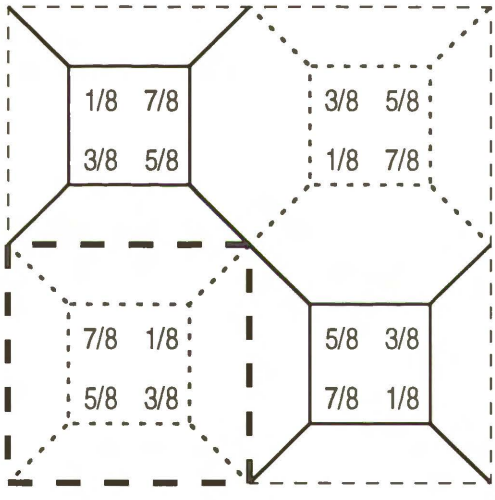

Figure 3.9: The schematic representation of the initial configuration used to create structures of symmetry of gyroid phase.

The tetrahedrons drawn in Fig. 3.7 and Fig. 3.8 with thick solid lines are the kaleidoscopic cells used to build the unit cell. The way of constructing the unit cell by replicating the kaleidoscopic cell is described in Section 3.8. One can easily see now, that in order to build the field in a unit cell on a small cubic lattice, $N = 3$, it is enough to specify the values of the field

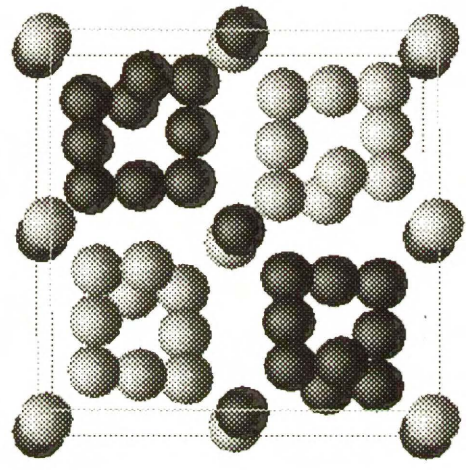

Figure 3.10: The initial configuration used to create structures of symmetry of gyroid phase.

$\phi(\mathbf{r}) = \phi_{i,j,k}$ only at the points inside the tetrahedrons. The values of the field at the remaining points can be set by using the symmetry of the structures. Thus instead of specifying $3^3 = 27$ values of $\phi_{i,j,k}$ one has to specify these values at four point of the cubic lattice for the simple cubic structure. Using this method in the case of double diamond structures gives even bigger gain, where it is sufficient to set the values of the field at five points in order to set up the field for a cubic lattice containing $5^3 = 125$ points.

The small lattice can be enlarged to desired size by changing the number of points from N to $2N - 1$ and finding the values of $\phi_{i,j,k}$ in new lattice sites by interpolation. Fig. 3.11 illustrates how the interpolation can be done. The hollow circles represent the values of the lattice mapped to the enlarged lattice. The values on the edges of the cube, represented by black

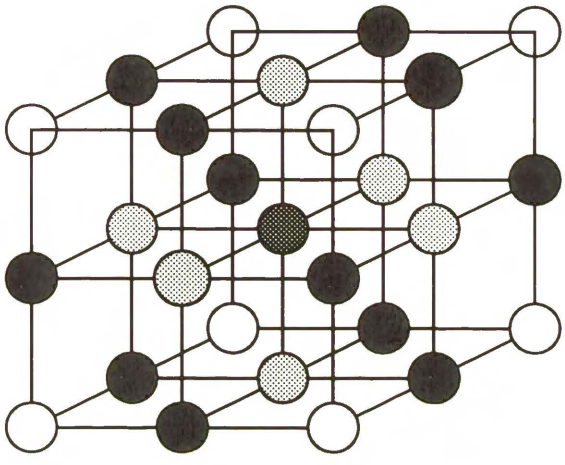

Figure 3.11: The illustration of interpolation done during enlarging the lattice size.

circles, are calculated by taking 1/2 of the sum of the values on vertices of the cube common with these edges. The values at the center of faces of the cube, represented by light grey circles, are computed as 1/4 of the sum of the values at the edges common with these faces. The value at the center of the cube is calculated as 1/6 of the sum of the values at the centers of the cube faces. There are of course other possibilities of doing the interpolation. The interpolation done to enlarge the lattice has no influence on the results. It may only speed up the calculations if it is done appropriately.

3.8 Symmetry

We impose on the field $\phi(\mathbf{r})$ the symmetry of the structure we are looking for by building up the field inside a unit cubic cell of a smaller polyhedron,

replicating it by reflections, translations, and rotations. These polyhedra are pictured with thick solid lines in Figs. 3.12, 3.14, 3.13. They are identical with the polyhedra described by Coxeter [37] as kaleidoscopic cells. Such a procedure not only guarantees that the field has required symmetry but also enables substantial reduction of independent variables $\phi_{i,j,k}$ in the function $F(\{\phi_{i,j,k}\})$.

The structures we have generated can be, in principle, characterized by space group symmetry [38, 39, 32] analogically to molecular crystals. The simple cubic structure has the space group $Im\bar{3}m$, double diamond $F\bar{4}3m$, gyroid $Ia\bar{3}d$. However this is not always obvious even for the structures of simple topology which Bravais lattice should be assign to a given structure [32]. For more complex structures assigning a Bravais lattice becomes not clear. Therefore we decided to characterize the symmetry of the structures, we have generated, by including it in the class of symmetry characteristic for the following structures: simple cubic, double diamond, and gyroid. All these structures belong to the class of cubic symmetry, thus here we generate only the structures belonging to this class.

The structures having the symmetry of the simple cubic phase are built of quadrirectangular tetrahedron replicating it by reflection, Fig. 3.12. The faces of the tetrahedron lie in the planes of mirror symmetry. The volume of the tetrahedron is 1/48 of the unit cell volume.

The structures of the double diamond phase symmetry are built in the following way. First the unit cell is divided into eight smaller cubes. The field in the one of the small cubes is built of trirectangular tetrahedron in the same

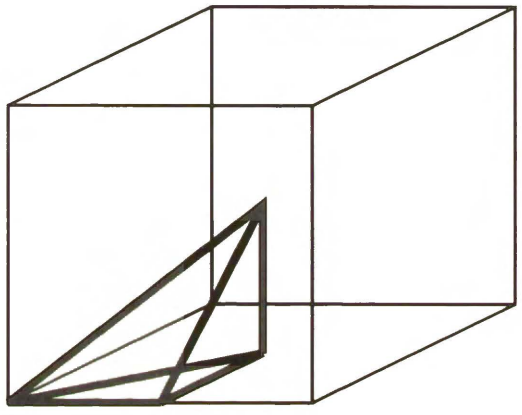

Figure 3.12: The thin solid lines show the unit cell. The thick solid lines show the kaleidoscopic cell used to create structures of simple cubic phase symmetry: the quadrirectangular tetrahedron. See Fig. 3.7.

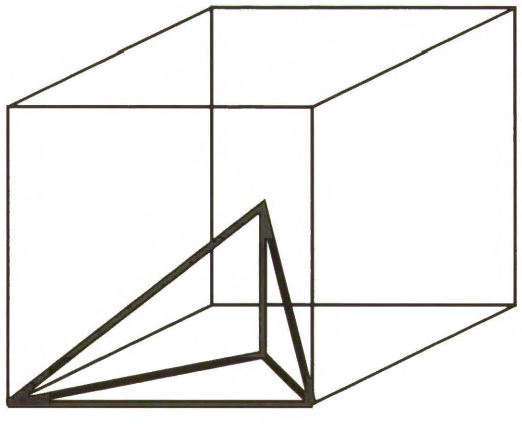

Figure 3.13: The thin solid lines show 1/8 of the unit cell. The thick solid lines show the kaleidoscopic cell used to create structures of double diamond phase symmetry: trirectangular tetrahedron. See Fig. 3.8.

way as in the previous case, Fig. 3.13. The volume of the tetrahedron is 1/24 of the unit cell volume. Next the field in the unit cell is build of this cube by translations and translations combined with a change of sign of the field from $\phi_{i,j,k}$ to $-\phi_{i,j,k}$. The cube with the field build of the tetrahedron is translated by the following vectors: $[L/2, L/2, 0]$, $[0, L/2, L/2]$, and $[L/2, 0, L/2]$. Next the sign of the field in the small cube is changed and the cube with such a different field is translated by the following vectors: $[0, 0, L/2]$, $[0, L/2, 0]$, $[L/2, 0, 0]$, and $[L/2, L/2, L/2]$. L in both cases is the unit cell length. Such a procedure enables reduction of the unit cell volume by a factor $1/(8*24) = 1/192$.

If the $\phi(\mathbf{r})$,$-\phi(\mathbf{r})$ symmetry is not applied the trirectangular tetrahedron can also be used to create the structures of double diamond phase symmetry. In such a case the cube shown in Fig. 3.13 as 1/8 of the unit cell becomes the unit cell. The unit cell volume is therefore reduced by the factor 1/24.

The structures of gyroid phase symmetry are built of rectangular parallelopiped, Fig. 3.14. It consists 1/16 of the unit cell volume. The parallelopiped is rotated by 90 degrees according to four fold screw rotation axis parallel to z direction, located at the point $\mathbf{r} = (L/4, L/4, L/4)$ and translated in the direction of z axis by the vector $[L/4, 0, 0]$. Repeating this operation three times fills out 1/4 of the unit cell volume with a new rectangular parallelopiped spanned by a vector $[L, L/2, L/2]$ located at the point $\mathbf{r} = (0, 0, 0)$. Next this new parallelopiped is rotated according to two fold rotation axis parallel to y direction and located at the point $\mathbf{r} = (L/2, 0, L/2)$. The parallelopiped created by this operation spanned by the vector $[L, L/2, L/2]$ located at the

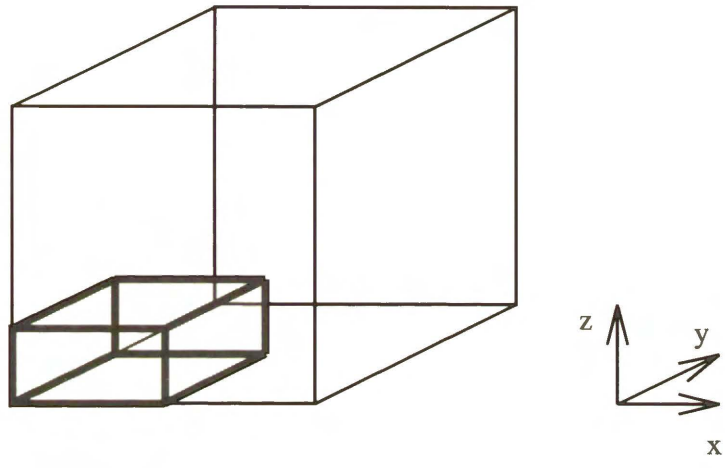

Figure 3.14: The thin solid lines show the unit cell. The thick solid lines show the kaleidoscopic cell used to create structures of gyroid phase symmetry: the parallelepiped. See Figs. 3.9, 3.10.

point $\mathbf{r} = (L/2, 0, 0)$ is translated by the vector $[-L/2, L/2, 0]$. The sign of the field in this parallelopiped is changed from $\phi_{i,j,k}$ to $-\phi_{i,j,k}$. After these transformation $1/2$ of the unit cell is recreated. The other half of the unit cell is created of the previous one by rotating it according to two fold rotation axis parallel to z direction and located at the point $\mathbf{r} = (L/2, L/2, 0)$.

3.9 Conjugate gradient method

We use conjugate gradient method [40] to minimize the function $F(\{\phi_{i,j,k}\})$. Minimization was done with respect to $\{\phi_{i,j,k}\}$ for a given value of the cell length $L = (N-1)h$. We have varied h to find the cell length for the lowest value of the free energy functional $F(\{\phi_{i,j,k}\})$. First we have done

the calculation for a small lattice size $N = 33$. The configuration obtained for the lattice size N was next used to produce the configuration for the bigger lattice size $2N - 1$. It was done by interpolation the values of the field $\phi(\mathbf{r}) = \phi_{i,j,k}$ from the small lattice to fill out the empty sites on the bigger lattice in the way described in Section 3.7.

The conjugate gradient method requires calculation of partial derivatives of the function $F(\{\phi_{i,j,k}\})$

$$\frac{\partial F(\{\phi_{l,m,n}\}, \phi_{l_1,m_1,n_1})}{\partial \phi_{l_1,m_1,n_1}} \tag{3.21}$$

where $\{\phi_{l,m,n}\}$ is the set of all variables of the function $F[\{\phi_{i,j,k}\}]$ except the variable ϕ_{l_1,m_1,n_1}. This derivative can be, in principle, calculated analytically. However, due to reduction of the unit cell volume (see for example Figs. 3.12, 3.13) these derivatives would have to be computed in a different way in different places of this volume, therefore the analytical calculation of the derivatives would require different formulas for these derivatives at the vertives, edges and faces. The analytical calculation of derivatives would also introduce some inconsistency to our calculations, because we calculate all other derivatives numerically. Fortunately, it does not imply the loss of accuracy, therefore the derivatives (3.21) are approximated in our calculations by

$$\frac{F(\{\phi_{l,m,n}\}, \phi_{l_1,m_1,n_1} + \Delta\phi) - F(\{\phi_{l,m,n}\}, \phi_{l_1,m_1,n_1})}{\Delta\phi} \tag{3.22}$$

where $\Delta\phi << \phi_{i,j,k}$. It is extremally important to code this part of the program efficiently. It may result in speeding up the program by few orders of magnitude if the number of variables $\phi_{i,j,k}$ is large. It is worth to note that the value of the expression (3.22) depends only on the values of ϕ_{l_1,m_1,n_1} its near neighbors and next near neighbors. Thus instead of calculating the values of the function $F(\{\phi_{i,j,k}\})$ in all lattice points it is sufficient to calculate these values only in a few points.

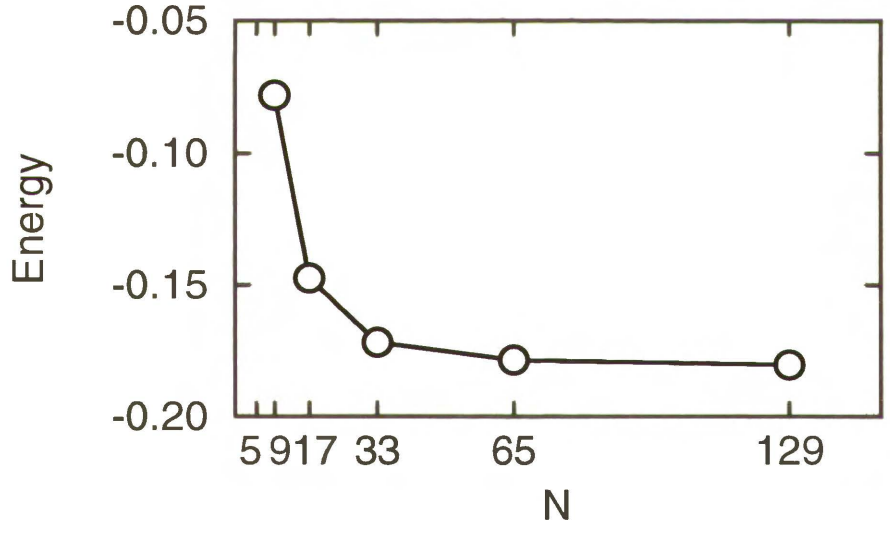

Figure 3.15: The free energy per unit volume for the simple cubic structure, calculated from the functional (2.9) for the parameters $f_0 = 0$ and $g_0 = 0$ as a function of the lattice size.

The solution for the discretized model of a continuous functional is obtained with certain accuracy. The accuracy depends on the value of the

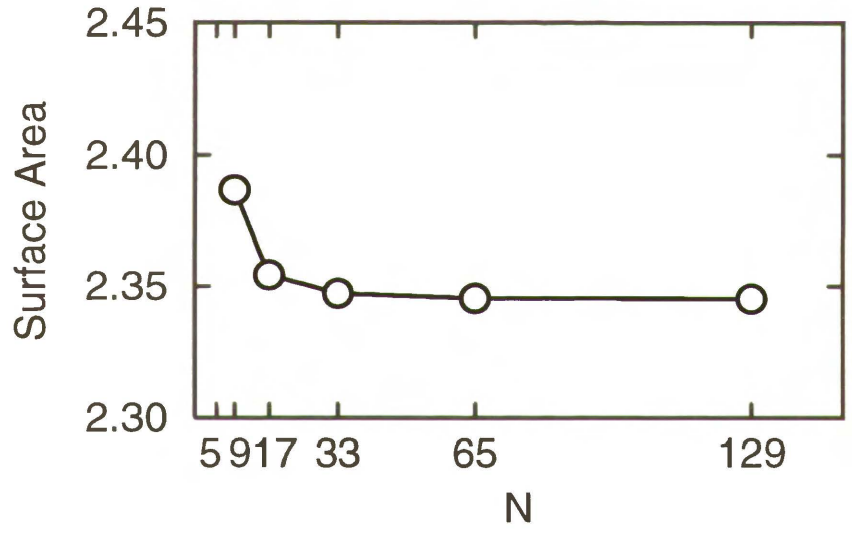

Figure 3.16: The normalized surface area per face of the unit cell of $\phi(\mathbf{r}) = 0$ for the simple cubic structure, calculated from the functional (2.9) for the parameters $f_0 = 0$ and $g_0 = 0$ as a function of the lattice size.

lattice spacing h and the number of points N. We have checked the accuracy of our results by calculating the free energy and the surface area of $\phi(\mathbf{r}) = 0$ for a few different sizes of the lattice. Fig. 3.15 shows that the free energy is very sensitive for the lattice size. We used in our calculations $N = 129$ which results in over 2 million points per unit cell. This value seems to give sufficient accuracy for the calculation of the free energy. For the calculation of the surface area of $\phi(\mathbf{r}) = 0$ smaller lattice can be used to obtain high accuracy. Fig. 3.16 shows that the values of the surface area of the internal interface change only slightly for $N = 33, 65, 129$.

Chapter 4

Results

We have generated lots of unknown structures as well as few known. Among the generated surfaces are the triply periodic minimal surfaces. These surfaces have been considered paradigms of the internal interface in the ordered phases formed in the mixtures containing surfactant. We describe these surfaces in Section 4.1. To the best of our knowledge the results we present are the first ones showing that a triply periodic minimal surface can be the solution of a physical model. In Section 4.2 we present unknown surfaces of low genus resulted from our model. We speculate that some of these surfaces can be new triply periodic minimal surfaces. The surfaces of high genus are presented in Section 4.3. The pictures of these surfaces strongly resemble the pictures of microemulsion taken during freeze fracture microscopy studies. In Section 4.4 we describe new type of structures, **the multiply continuous ones.** Our discovery calls for new experiments confirming or rejecting the existence of such structures in real systems (so far only bicontinuous struc-

tures have been considered). The phase diagram of the model is presented in Section 4.5.

4.1 Minimal Surfaces

The following simple experiment can be used for the direct visualization of a simple patch of minimal surface: Take a metal non-planar frame and immerse it in the water solution of soap. The soap bubble which forms on this frame assumes the shape that minimizes its surface free energy associated with the surface tension and consequently it forms a surface of least area. Thus these surfaces are called minimal surfaces. Such experiments can be traced back to Leonardo da Vinci but in fact the detailed studies of this type were done and published by Plateau [41] and hence later the problem of surface of least area spanning a given loop has been named the Plateau problem.

The history of physics and mathematics of minimal surfaces ran in parallel. Lagrange in 1761 (before Plateau) derived the equations for a surface of least area that is equivalent to the condition of vanishing mean curvature at every point on the surface. The representation of these surfaces in terms of harmonic functions was given by Weierstrass in 1866 and this representation has served many researchers up to date for their generations. A new qualitative insight into the mathematics of the problem was obtained by Schwarz and his student Neovius, who showed that simple patches of minimal surfaces can be put together to give smooth periodic three dimensional structures, which are called now triply periodic minimal surfaces (TPMS)

or sometimes infinite periodic minimal surfaces (IPMS). They identified five phases three of which were of the cubic symmetry i.e. P, D and C(P). Plateau and Schwarz in fact entertained scientific contacts, but none of them had envisaged the role of these surfaces as physical interfaces. Rediscovery of the problem is due to Schoen [39], who identified 4 new surfaces of cubic symmetry(G, I-WP, F-RD and O,C-TO). In 1976 Scriven [42] hypothesized that such surfaces could be used for the description of physical interfaces appearing in ternary mixtures of water, oil and surfactants. In 1967/68 Luzzati et al [43, 44, 45, 46] observed this type of ordering in the lecithin-water and lipid-water systems. One of the phases observed by them was the phase of the same symmetry as the G Schoen minimal surface. It seems that both Schoen's and Luzzati discovery were made independently. In fact this phase appears to be very common in biological systems. Another example of such surfaces is found in the system of diblock copolymers, commercially important materials for the production of plastics. AB diblock copolymer consists of two macromolecules chemically bonded together. At low temperatures the system forms ordered A-rich and B-rich domains, with the points of bondage at the interface between the domains. In 1988 Thomas et al [47] observed that the PS/PI (polystyrene/polyisoprene) diblock copolymer forms a structure of the same symmetry as the D (diamond) Schwarz surface and argued on the basis of the relative volume fraction of PS and PI component that the resulting physical interface must be the surface of constant mean curvature at every point of the surface. Such surface belongs to the family of minimal surfaces [39, 32, 48].

Surfaces are ubiquitous. Even in the ionic crystals one can imagine a periodic zero potential surfaces (POPS in short), having same symmetry as the crystal [49]. Although, POPS do not have usually the same geometry as minimal surfaces (their mean curvature varies along the surface), nonetheless they share the same topology (genus etc) and symmetry as the latter.

The minimal surfaces are usually described in terms of Weierstrass integral equations. The Weierstrass representation gives the coordinates (x, y, z) on a minimal surface of the point represented by ω on the complex plane [50]

$$\begin{aligned} x &= Re \int_{\omega_0}^{\omega_1} (1-\omega^2) R(\omega) d\omega, \\ y &= Re \int_{\omega_0}^{\omega_1} i(1+\omega^2) R(\omega) d\omega, \\ z &= Re \int_{\omega_0}^{\omega_1} 2\omega R(\omega) d\omega, \end{aligned} \tag{4.1}$$

where $R(\omega)$ is the Weierstrass characteristic function for the surface, Re stands for "real part", $\omega = \omega_a + i\omega_b$ and $i = \sqrt{-1}$. When the function $R(\omega)$ is replaced with $R(\omega)e^{i\theta}$ the surface described by the function $R(\omega)$ is transformed into another surface called the adjoint surface. Such transformation is called the Bonnet transformation [51] and θ is known as the Bonnet angle. The Bonnet transformation preserves the Gaussian and mean curvatures.

4.1.1 Schwarz surfaces D, P and Schoen surface G

The Schwarz primitive surface P and Schoen gyroid surface G are related to the D-surface by the Bonnet transformation: the Bonnet angle for the P-surface is 90° and for the G-surface is 38.015°. The Weierstrass function for the fundamental element of the surfaces D is given by [50, 52]

$$R(\omega) = (\omega^8 - 14\omega^4 + 1)^{-1/2}, \tag{4.2}$$

with an integration domain given by the points around the origin limited by 4 circles with radius $\sqrt{2}$ and centers at $\pm\sqrt{2}, \pm i\sqrt{2}$.

Here we use our model to generate surfaces. The fact that the P,D,G surfaces are adjoint means that the histograms of the Gaussian curvature for these surfaces should be the same. In fact the histograms look very similar (see Figs. 4.6, 4.10, 4.14), the small differences result form the numerical accuracy. The mean curvature of the minimal surface is zero at every point, thus its histogram should be a single infinitely sharp peak at $H = 0$. Here it is smeared (see Figs. 4.7, 4.11, 4.15) due to numerical accuracy. In fact it serves as a good estimate of the errors for curvatures.

It is interesting that the value of the free energy in our model (2.9) for each of these structures is the lowest for all the structures of given symmetry, i.e. among all structures of the symmetry of gyroid phase G, this phase has the lowest free energy. These phases are generated independently of the initial configuration, provided that the unit cell length is set close to the minimal

length. If the cell length is taken close to multiple length of of the unit cell then multiple images of a given structure are created.

The fact that the G and D structures are the most stable among structures of a given symmetry suggest that they can be found in real system. In fact the phases, diamond D and gyroid G, have been discovered in real systems in diblock copolymers [47, 53, 54, 55, 56]. However, the discovery of the gyroid phase, after the diamond phase had been found real systems, was not straighforward. It took the researchech about six years to find the gyroid phase.

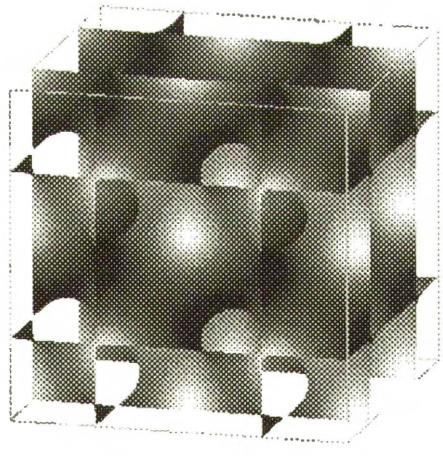

Figure 4.1: Schwarz diamond surface D generated from the functional (2.9). The unit cell. Off front view.

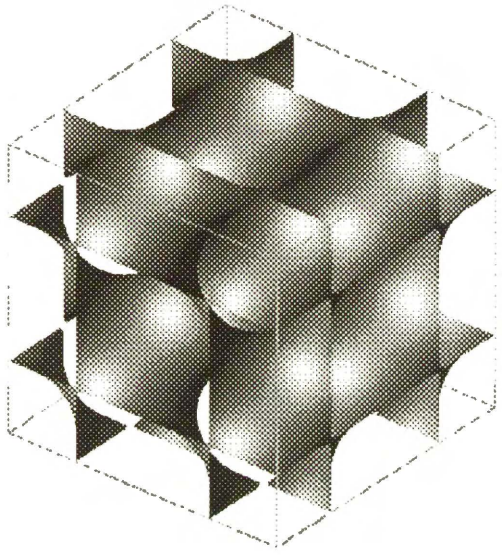

Figure 4.2: Schwarz diamond surface D generated from the functional (2.9). The unit cell. Off diagonal view.

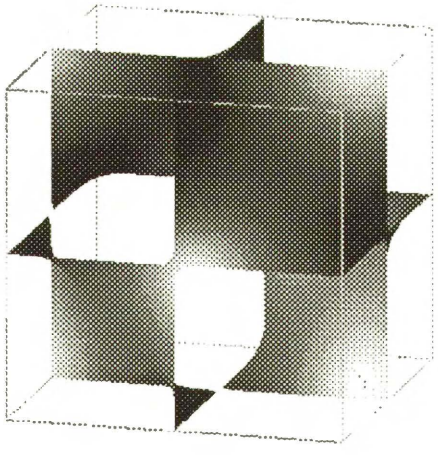

Figure 4.3: Schwarz diamond D surface generated from the functional (2.9) 1/8 of the unit cell. Off front view.

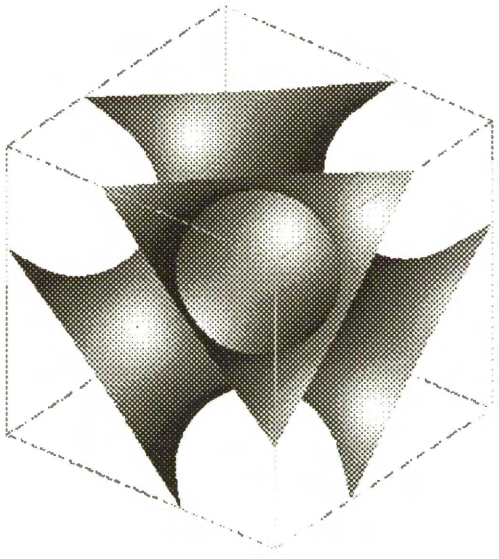

Figure 4.4: Schwarz diamond surface D generated from the functional (2.9) The middle element of the unit cell. Off diagonal view.

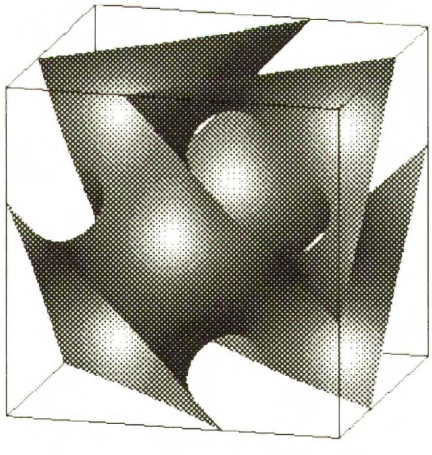

Figure 4.5: Schwarz diamond surface D generated from the functional (2.9) The middle element of the unit cell. Off front view.

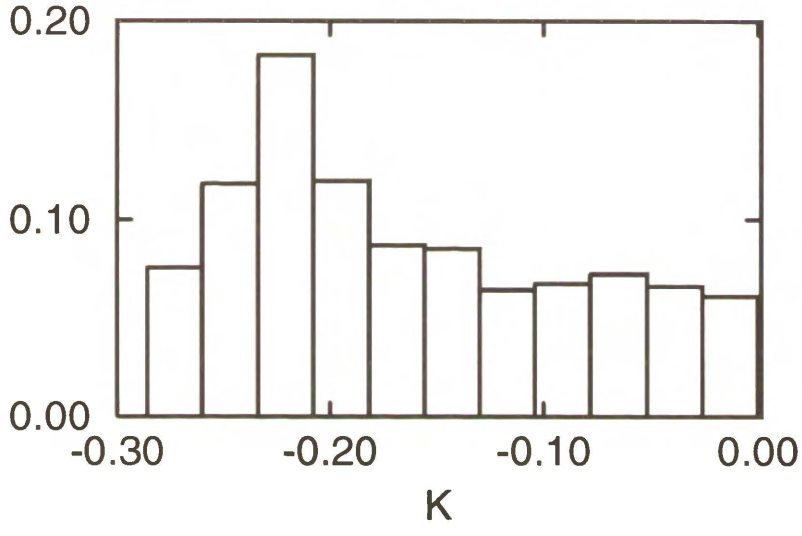

Figure 4.6: The histogram of the Gaussian curvature for the surface D

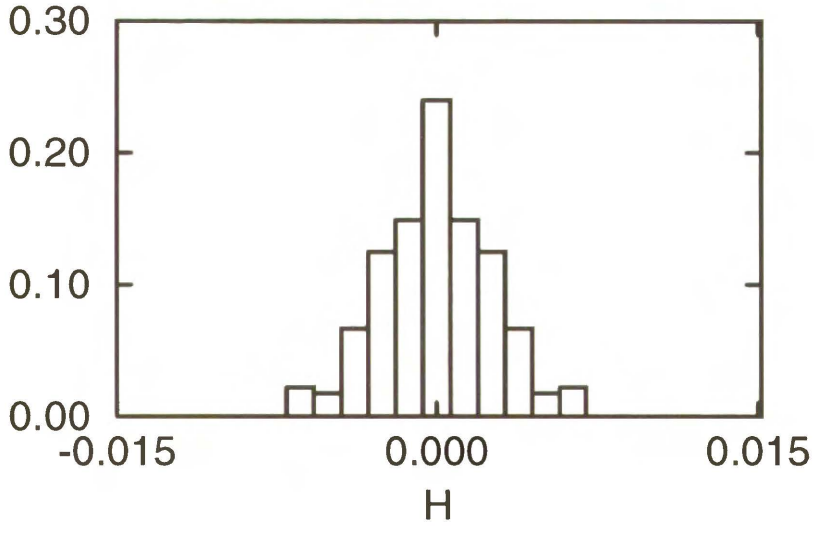

Figure 4.7: The histogram of the mean curvature for the surface D

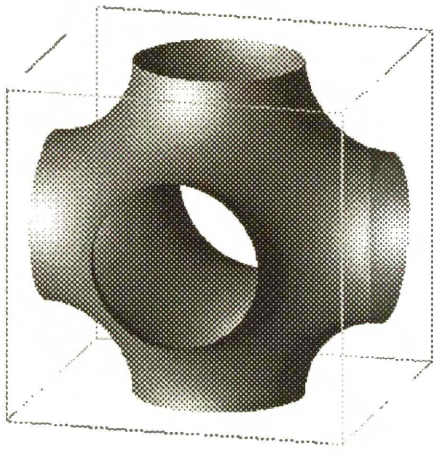

Figure 4.8: Schwarz surface P generated from the functional (2.9). The unit cell. Off front view.

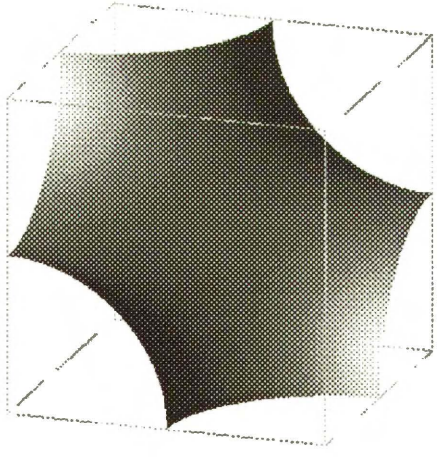

Figure 4.9: Schwarz primitive surface P generated from the functional (2.9) 1/8 of the unit cell. Off front view.

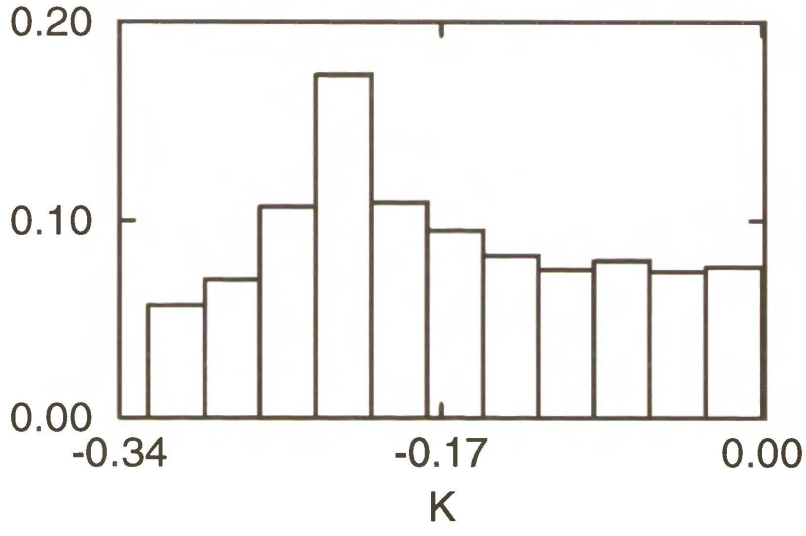

Figure 4.10: The histogram of the Gaussian curvature for the surface P

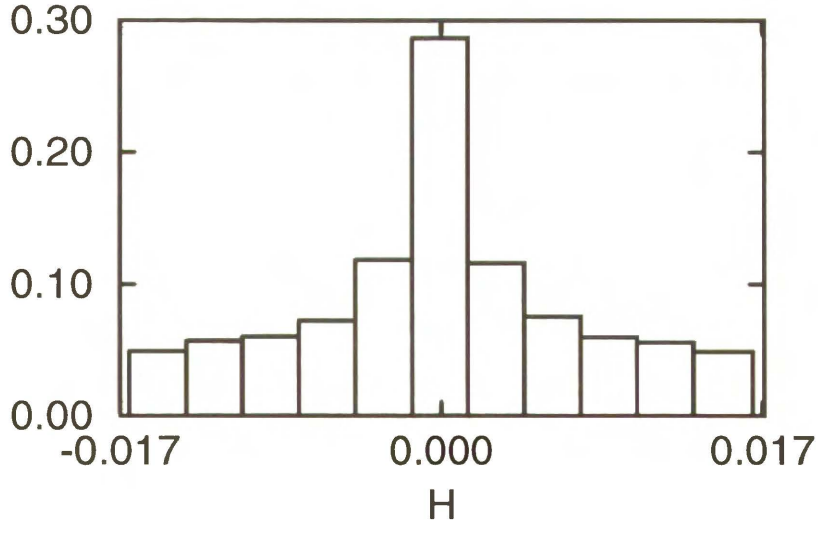

Figure 4.11: The histogram of the mean curvature for the surface P

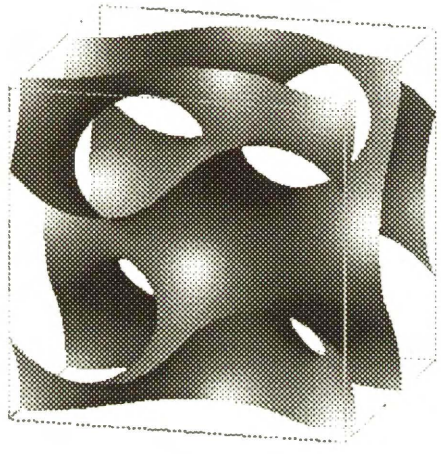

Figure 4.12: Schoen gyroid surface G generated from the functional (2.9) The unit cell. Off front view.

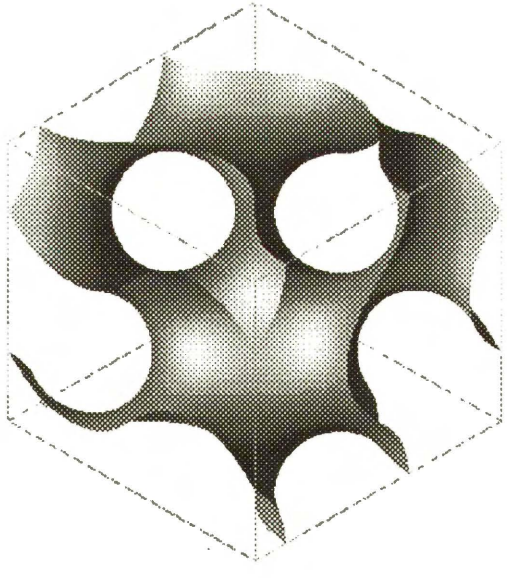

Figure 4.13: Schoen gyroid surface G generated from the functional (2.9) The unit cell. Off diagonal view.

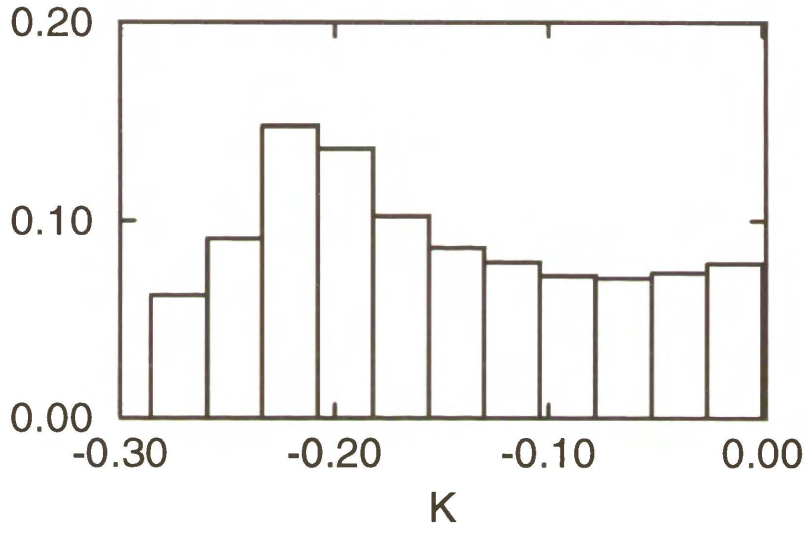

Figure 4.14: The histogram of the Gaussian curvature for the surface G

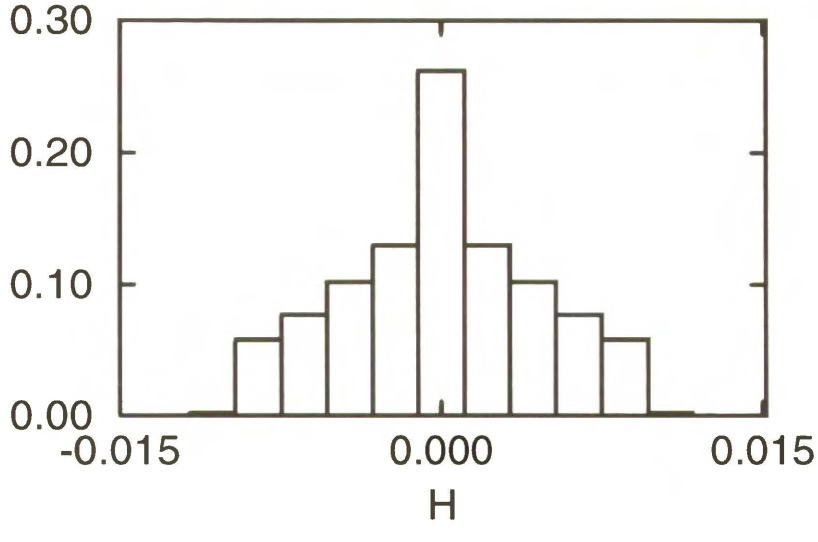

Figure 4.15: The histogram of the mean curvature for the surface G

4.1.2 Schoen I-WP and O,C-TO minimal surface

The I-WP surface was discovered by Schoen [39]. He built the models of the surface, identified its space group as $Im\bar{3}m$. That is why the letter I is in the first part of the name given by him to this surface. The WP stands for "wrapped package" because of the resemblance of finite portions of the graph to the arrangement of string on a simply wrapped package. The Weierstrass characteristic function for I-WP surface is [51, 57]:

$$R(\omega) = (\omega^6 - 5\omega^4 - 5\omega^2 + 1)^{-2/3} \tag{4.3}$$

The I-WP surface was found in star block co-polymers [58]. The results of our study suggest that it can also be found in the ternary surfactant mixtures.

The O,C-TO surface was discovered by Schoen [39]. The Weierstrass function for this surface is not known and no other information except genus and the symmetry are described in the literature. Here we report for the first time the volume fraction of the two subvolumes divided by the OCTO surface, see Table 4.1. Nobody so far has shown the existence of this structure in real systems. The surface obtained from the functional (2.9) strongly resembles the one described by Schoen. The histogram of the mean curvature suggest that this surface can be minimal. However, this is the only structure which cannot be minimized with respect to the cell length. For all structures except this one we were able to find the minimal cell length, i.e. varying the cell length we were able to find such length for which the free energy density of

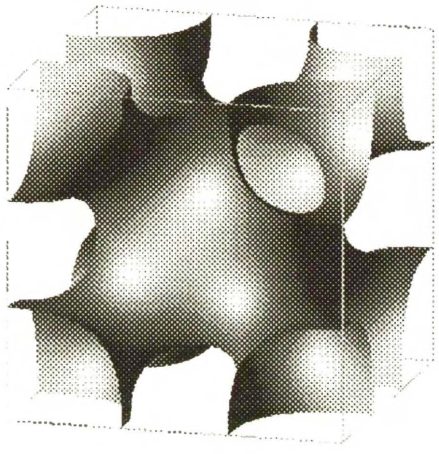

Figure 4.16: Schoen surface I-WP generated from the functional (2.9) The unit cell. Off front view.

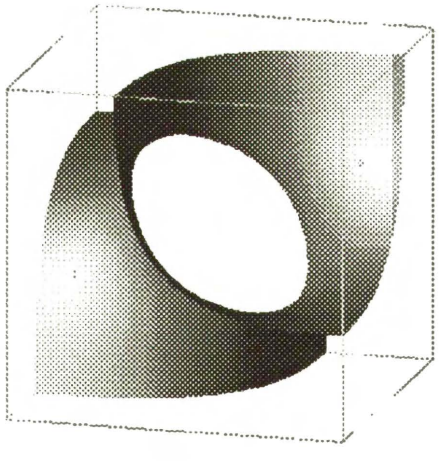

Figure 4.17: Schoen surface I-WP generated from the functional (2.9) 1/8 of the unit cell. Off front view.

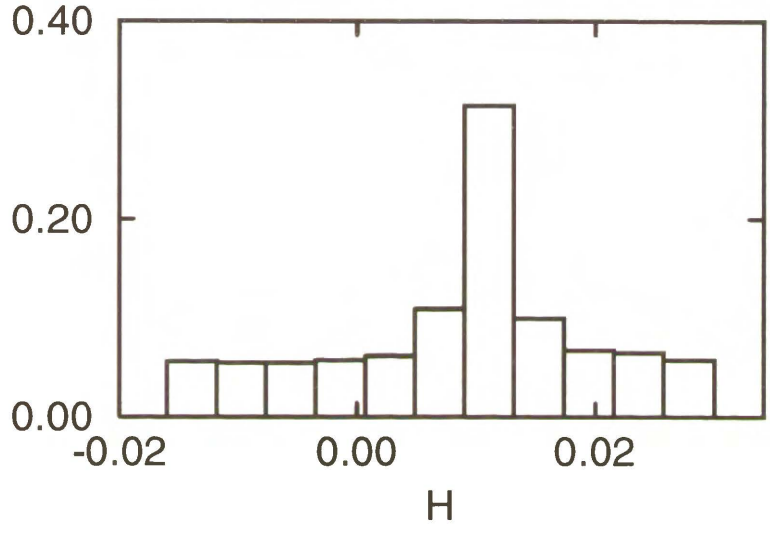

Figure 4.18: The histogram of the mean curvature for the surface I-WP

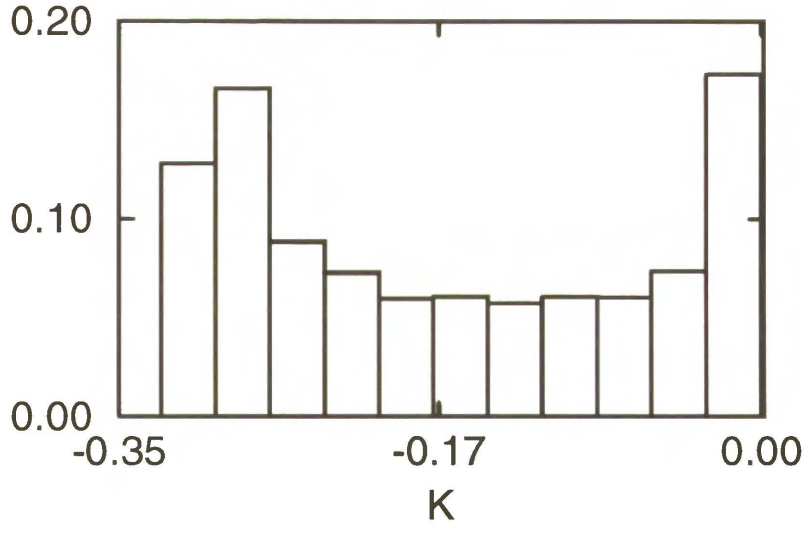

Figure 4.19: The histogram of the Gaussian curvature for the surface I-WP

the functional (2.9) is in minimum. The O,C-TO structure collapses to I-WP when the cell length is varied. Such a behavior suggests that this structure is very unstable and finding it in real systems is problematic.

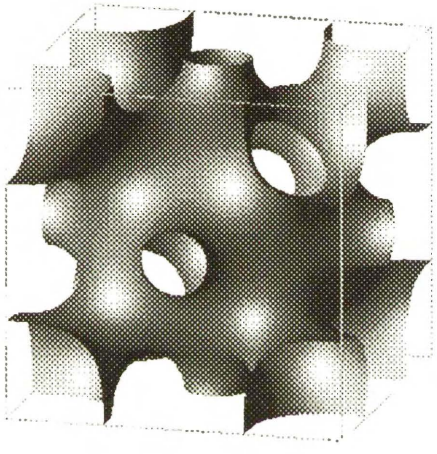

Figure 4.20: Schoen surface O,C-TO generated from the functional (2.9) The unit cell. Off front view.

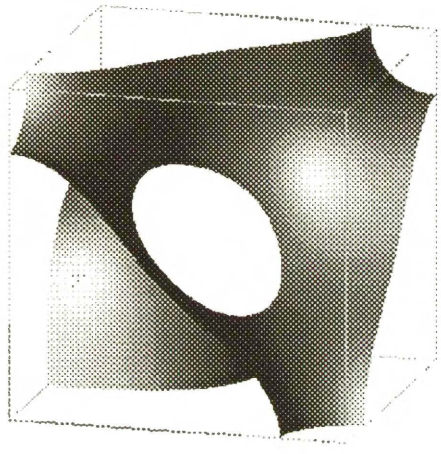

Figure 4.21: Schoen surface O,C-TO generated from the functional (2.9) 1/8 of the unit cell. Off front view.

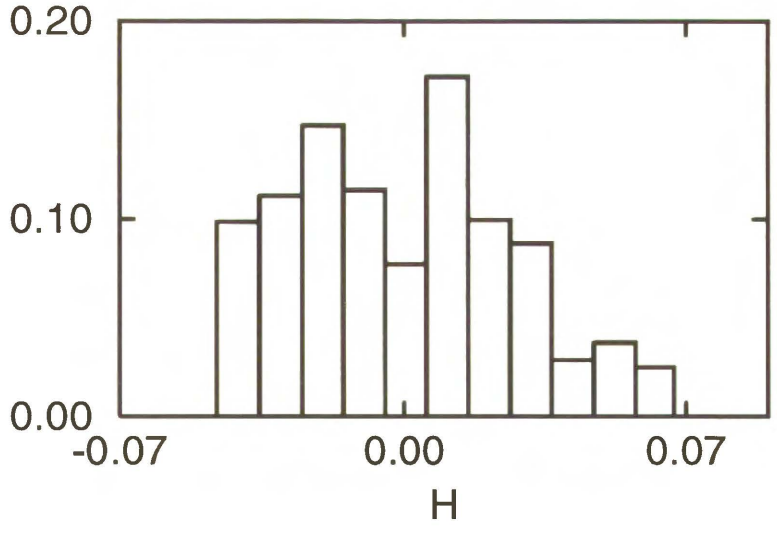

Figure 4.22: The histogram of the mean curvature for the surface O,C-TO

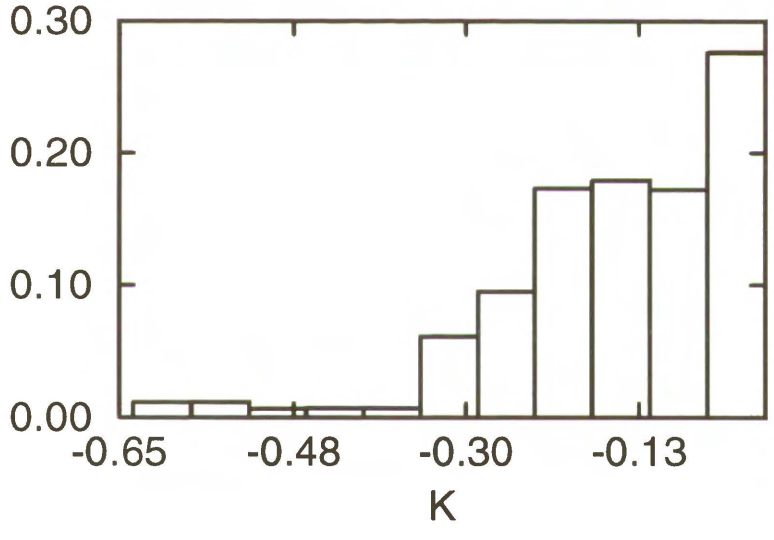

Figure 4.23: The histogram of the Gaussian curvature for the surface O,C-TO

Name	Cell Length	Energy	Surface Area	Genus	Volume Fraction
P	7.88	-0.181	2.3453 [2.3451068]	3	0.5
D	12.56	-0.188	3.8387 [3.8377862]	9	0.5
I-WP	11.78	-0.180	3.4640 [3.4646016]	7	0.533
G	10.08	-0.190	3.0919	5	0.5
O,C-TO	14.68	-0.162	3.6805	10	0.535

Table 4.1: The geometrical properties of the known minimal surfaces obtained from the functional (2.9), for the parameters $f_0 = 0.0$, $g_0 = -3.0$. In the square brackets are given the exact values found in the literature. Surface area $\tilde{S}$, in the table, is the normalized per face of the unit cube L^2 surface area S of the interface in the unit cell, $\tilde{S} = S/L^2$, $L = (N-1)h$. The energy is given per unit volume.

4.2 Low genus surfaces

In this section we present several examples of low genus surfaces of different symmetry: BFY, CPD, GP, DDU, GM. Very interesting are the BFY and CPD surface. They are of the same symmetry as the Schwarz P surface. The BFY surface can be generated from an arbitrary initial configuration if the length of the unit cell is set close to the equilibrium length, i.e. the length for the minimum of the functional (2.9). The pattern cut out on the face of the unit cell for BFY surface resembles "butterfly" wings. That is why we have given the symbol BFY to this surface as a abbreviation for "butterfly". It is remarkable that the volume fraction for BFY structure is 0.5.

The volume fraction for the CPD is not equal to 0.5, as it is in the case of I-WP and O,C-TO structures. CPD surface is very similar to the minimal surface discovered by Neovius [39, 32]. The difference is such that CPD surface has a hole inside a unit cell, therefore its genus is bigger. The histograms of the mean curvature for BFY and CPD surfaces suggest that they can be minimal, Figs 4.26, 4.30.

Very interesting histogram has the GP surface, Fig. 4.35. This is the structure of gyroid phase symmetry. The histogram of the mean curvature for GP surface is peaked at $H = 0$ as it is for minimal surfaces, but it has also two symmetric peaks at $H \neq 0$. It rather cannot be attributed to the numerical errors, because this surface has low genus ($g = 21$) and thus should be calculated with high accuracy.

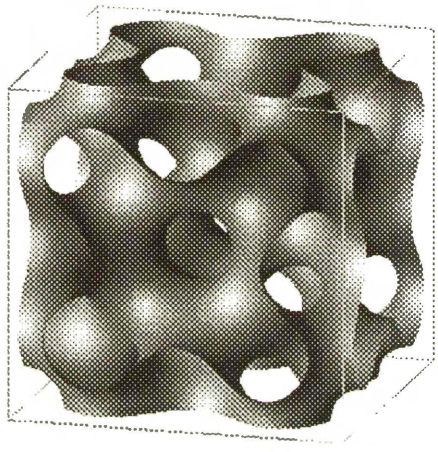

Figure 4.24: BFY surface generated from the functional (2.9). The unit cell. Off front view.

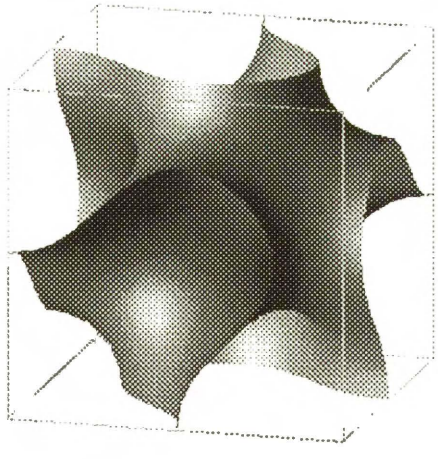

Figure 4.25: BFY surface generated from the functional (2.9). 1/8 of the unit cell. Off front view.

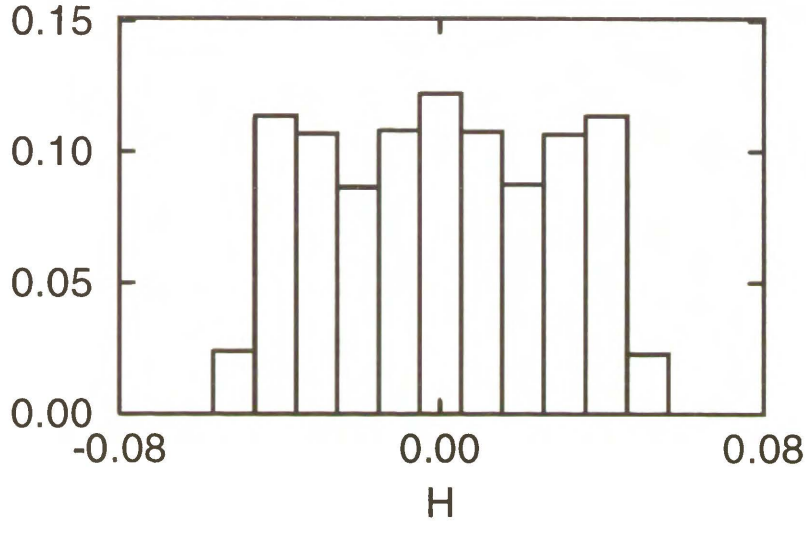

Figure 4.26: The histogram of the mean curvature for the surface BFY

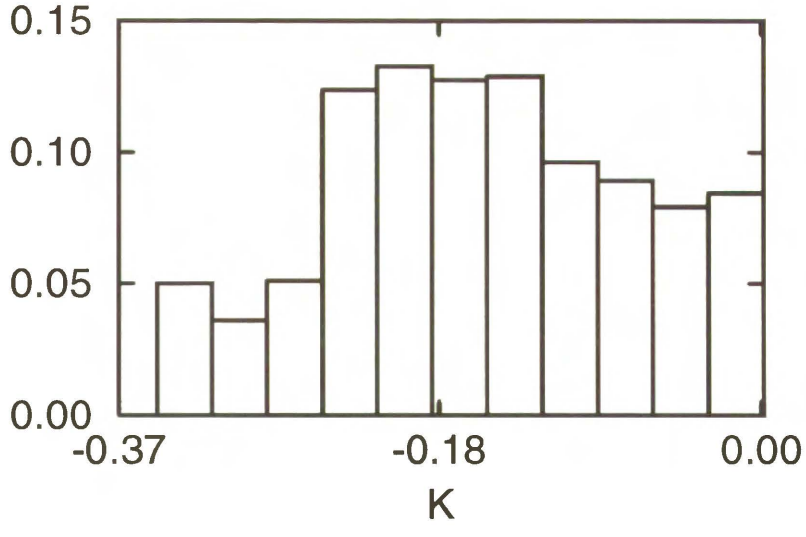

Figure 4.27: The histogram of the Gaussian curvature for the surface BFY

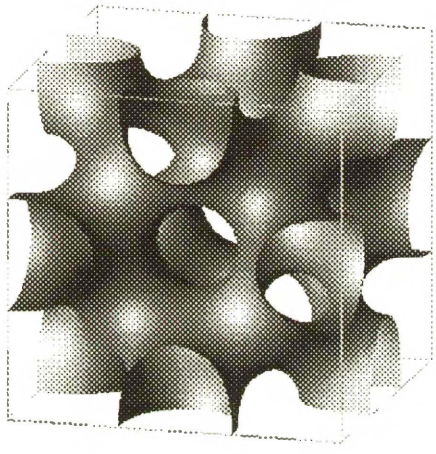

Figure 4.28: CPD surface generated from the functional (2.9). The unit cell. Off front view.

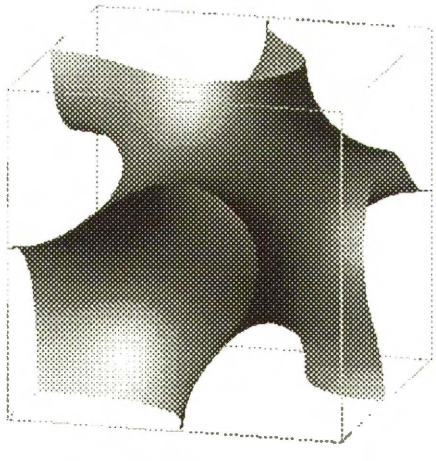

Figure 4.29: CPD surface generated from the functional (2.9). 1/8 of the unit cell. Off front view.

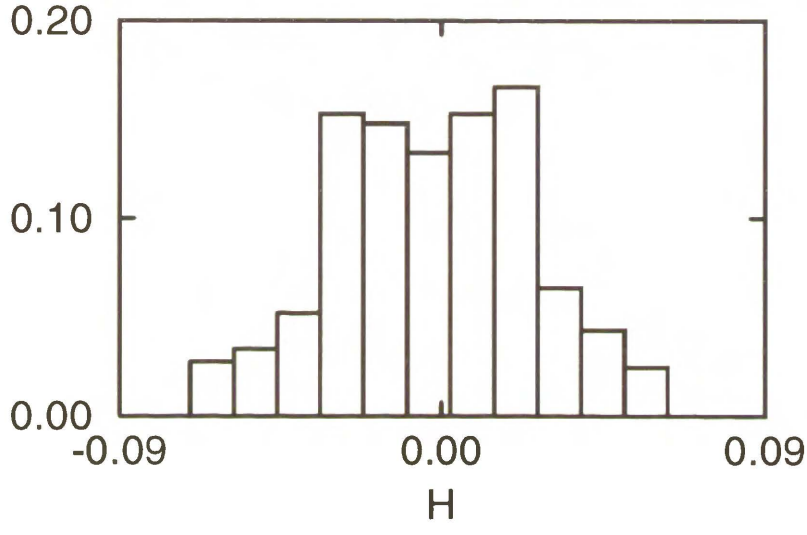

Figure 4.30: The histogram of the mean curvature for the surface CPD

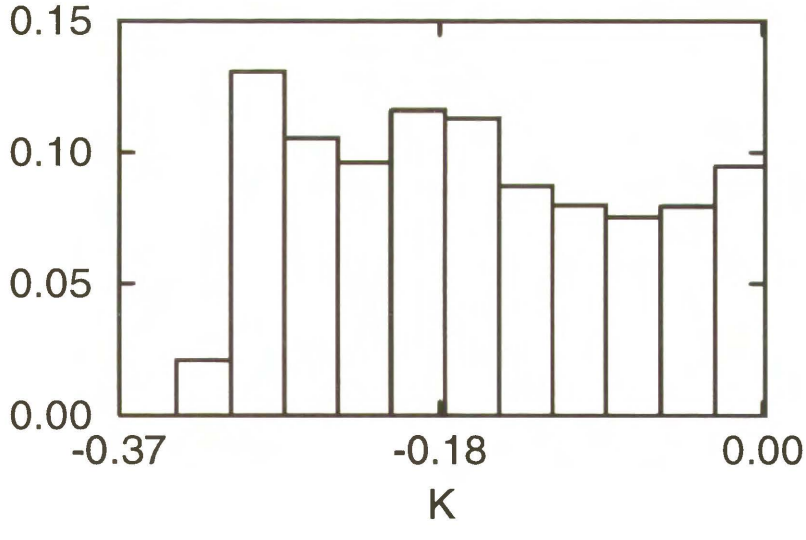

Figure 4.31: The histogram of the Gaussian curvature for the surface CPD

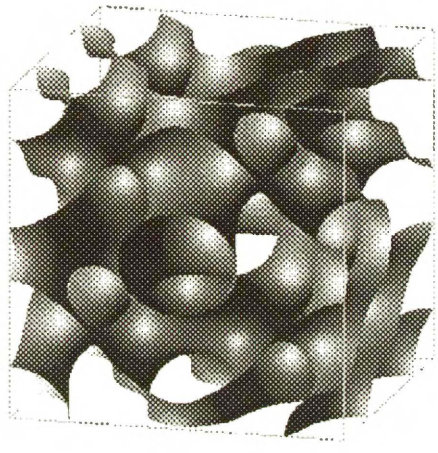

Figure 4.32: GP surface generated from the functional (2.9). The unit cell. Off front view.

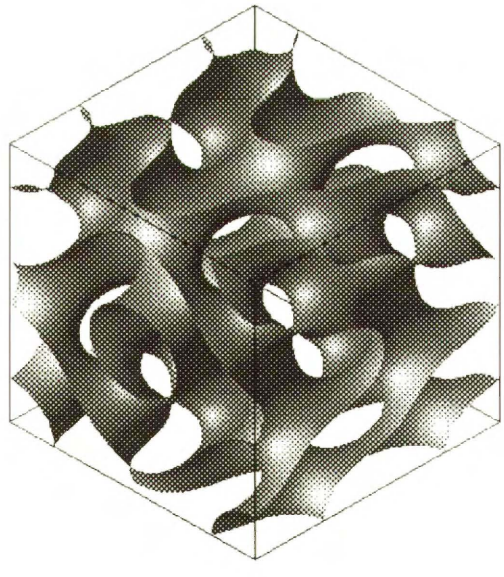

Figure 4.33: GP surface generated from the functional (2.9). The unit cell. Off diagonal view.

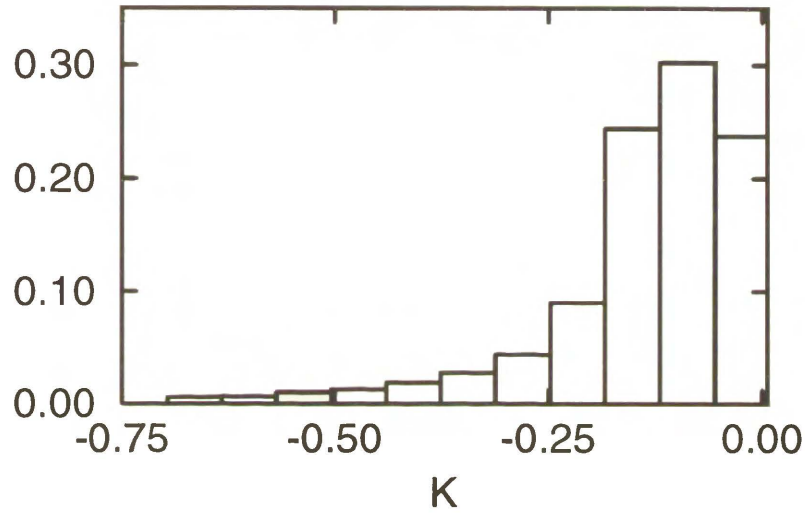

Figure 4.34: The histogram of the Gaussian curvature for the surface GP

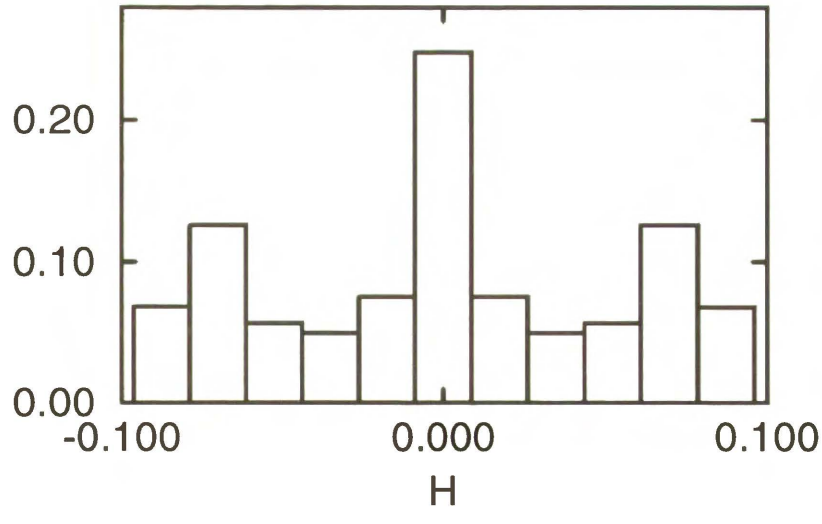

Figure 4.35: The histogram of the mean curvature for the surface GP

The structures GM and DDU are generated of trirectangular tetrahedron, see Fig. 3.13, i.e. in a similar way as the double diamond phase. The difference is such that 1/8 of the unit cell for the double diamond phase is a unit cell for the structures DDU and GM. The topology of the DDU structure is similar to the topology of the double diamond D structure. It can be seen by comparing the unit cell for DDU, Fig. 4.37, and the middle element of the double diamond structure D, Fig. 4.4. Thus it is rather unlikely that the DDU surface is minimal. This is also confirmed by the histogram of the mean curvature, Fig. 4.40. Although the DDU surface is not minimal it does not mean that the DDU structure cannot be found in real systems. In the scattering experiments one can investigate the symmetries of the structures, and on such basis one can guess the properties of the surfaces found in a given structure. The DDU structure was not known so far, and nobody considered its existence in real systems.

The GM structure is a combination of the Schwarz P surface, Fig. 4.8, and DDU surface. This surface as the DDU one also should not be minimal, see Fig. 4.46 The structures DDU and GM are not symmetric, i.e the volume fraction of oil and water is not equal to 0.5. The cubic cell for GM and DDU contains a few not connected pieces of the surface $\phi(\mathbf{r}) = 0$. However the whole surface is continuous. We have collected 8 cubic unit cells and shown in Figs. 4.38, 4.39, 4.44, 4.45 to illustrate how the infinite continuous triply periodic surface is built of the cubic unit cell.

Whether new surfaces we have generated are minimal or not is an interesting question. On the basis of numerical analysis we can speculate that

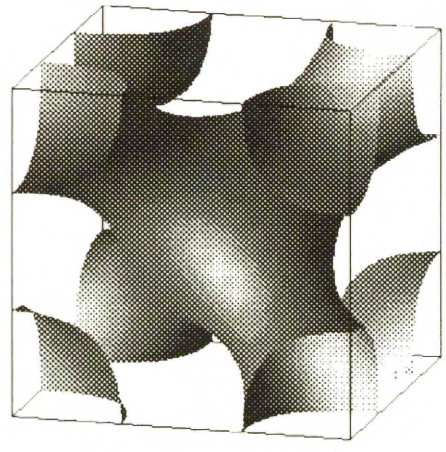

Figure 4.36: DDU surface generated from the functional (2.9). The unit cell. Off front view.

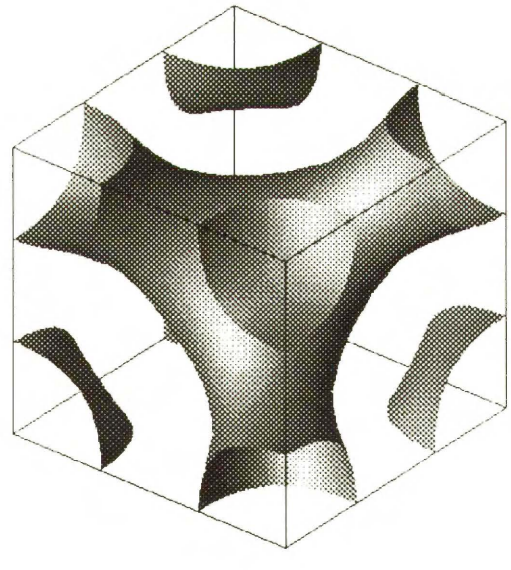

Figure 4.37: DDU surface generated from the functional (2.9). The unit cell. Off diagonal view.

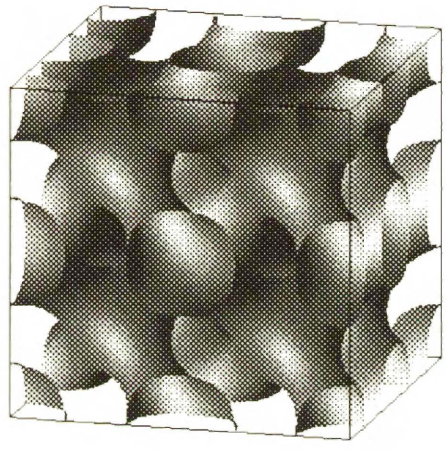

Figure 4.38: DDU surface generated from the functional (2.9). 8 unit cells. Off front view.

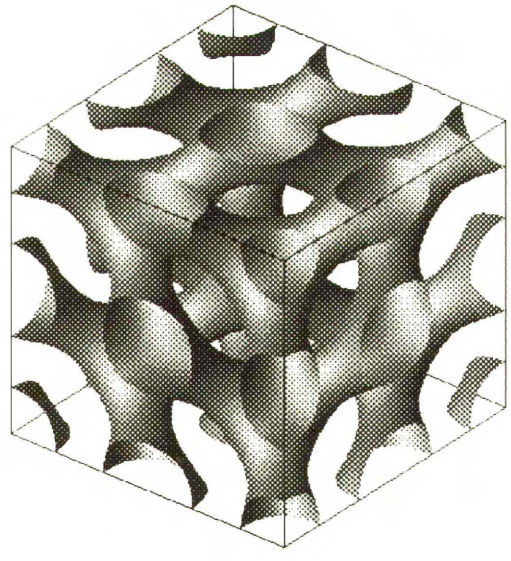

Figure 4.39: DDU surface generated from the functional (2.9). 8 unit cell. Off diagonal view.

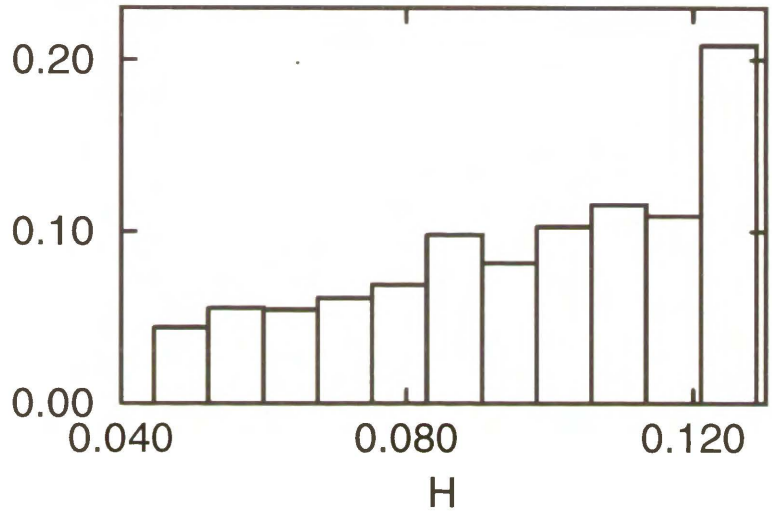

Figure 4.40: The histogram of the mean curvature for the surface DDU

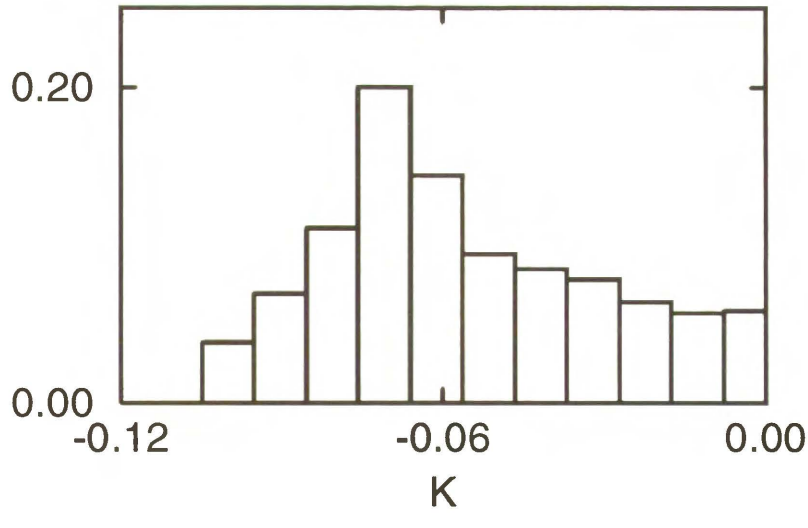

Figure 4.41: The histogram of the Gaussian curvature for the surface DDU

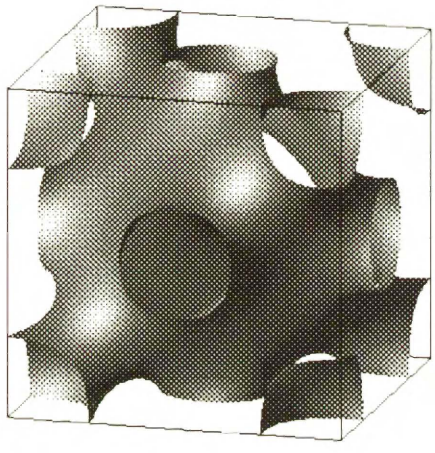

Figure 4.42: GM surface generated from the functional (2.9). The unit cell. Off front view.

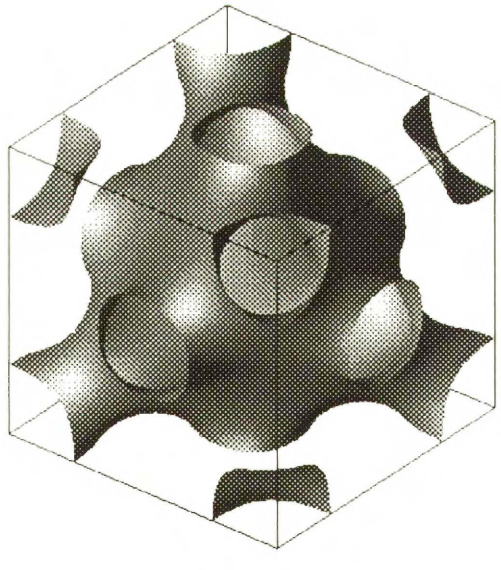

Figure 4.43: GM surface generated from the functional (2.9). The unit cell. Off diagonal view.

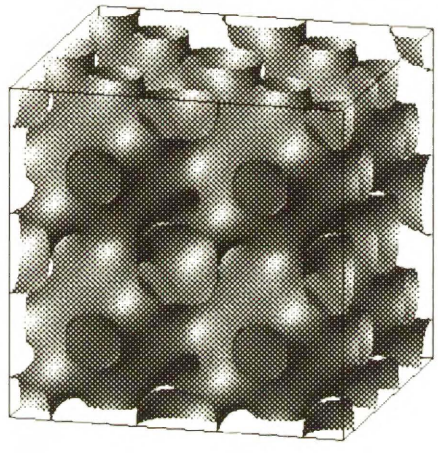

Figure 4.44: GM surface generated from the functional (2.9). 8 unit cells. Off front view.

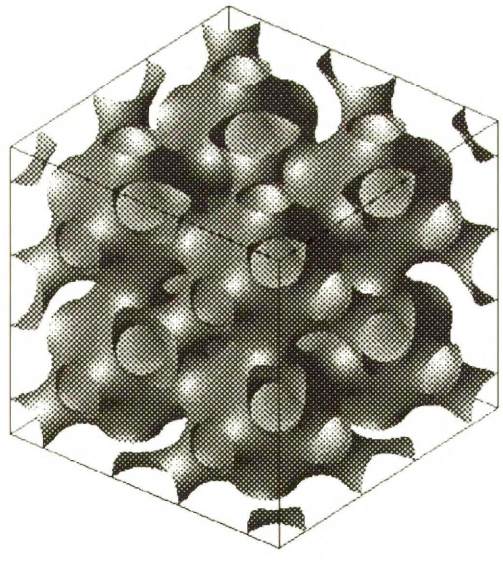

Figure 4.45: GM surface generated from the functional (2.9). 8 unit cells. Off diagonal view.

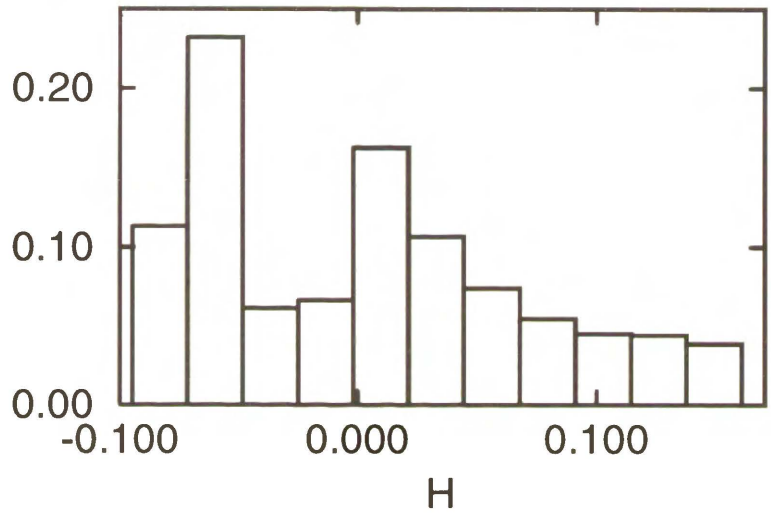

Figure 4.46: The histogram of the mean curvature for the surface GM

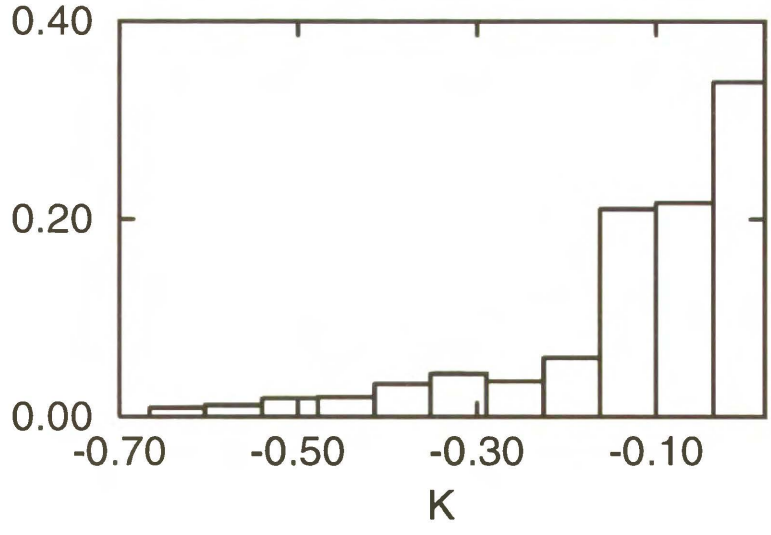

Figure 4.47: The histogram of the Gaussian curvature for the surface GM

Name	Cell Length	Energy	Surface Area	Genus	Volume Fraction
CPD	15.2	-0.174	4.3588	14	0.515
BFY	16.7	-0.180	4.9641	19	0.5
DDU	23.04	-0.181	3.2972	3	0.529
GM	24.00	-0.176	3.4925	6	0.520
GP	18.32	-0.183	5.4840	21	0.5

Table 4.2: The geometrical properties of low genus surfaces obtained from the functional (2.9), for the parameters $f_0 = 0.0$, $g_0 = -3.0$. Surface area $\tilde{S}$, in the table, is the normalized per face of the unit cube L^2 surface area S of the interface in the unit cell, $\tilde{S} = S/L^2$, $L = (N-1)h$. The energy is given per unit volume.

many of these surfaces are minimal. However, the definite answer is left to mathematicians, which have investigated the problem of minimal surfaces for over 100 years. We are more interested in the physics of the problem and in general in obtaining new undiscovered periodic surfaces (not necessarily minimal). Certainly not all of the generated surfaces are minimal e.g. GP, DDU, GM (see the mean curvature histograms).

4.3 High genus embedded periodic surfaces

The high genus surfaces are most easily generated for the values of parameters f_0 and g_0 in (2.9) taken near the boundary of lamellar and microemulsion phase and for the bigger unit cell length, $L = (N-1)h$, than the length of structures of low genus. This suggest the the microemulsion can be considered as a bicontinuous structure of high genus surface. These are only speculations based on theoretical studies. New experiments are needed to check these speculations. We hope that our results will help experimentalists to design such experiments.

We present in this chapter several examples of high genus surfaces of different symmetry. The structure CD has the symmetry of double diamond phase, the structure SCN1 has the symmetry of the simple cubic phase, and the structures GX1,GX2, GX3, GX5, GX6, GX7 have the gyroid phase symmetry.

The CD structure is especially interesting, because it has the same symmetry as the Schwartz diamond D phase. It has been generated in the same way as the diamond D phase, that is we have reduced the unit cell by a factor 1/192. Having done such a reduction we hardly expected the possibility of generation of a new surface. In fact, enlarging the length of the cubic cell we usually have got the multiple replicas of the diamond D structure, except the case when CD structure was generated.

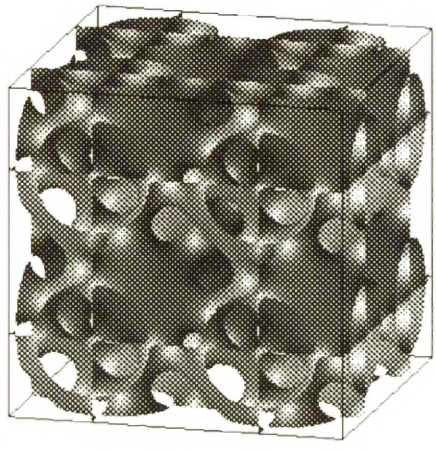

Figure 4.48: CD surface generated from the functional (2.9). The unit cell. Off front view.

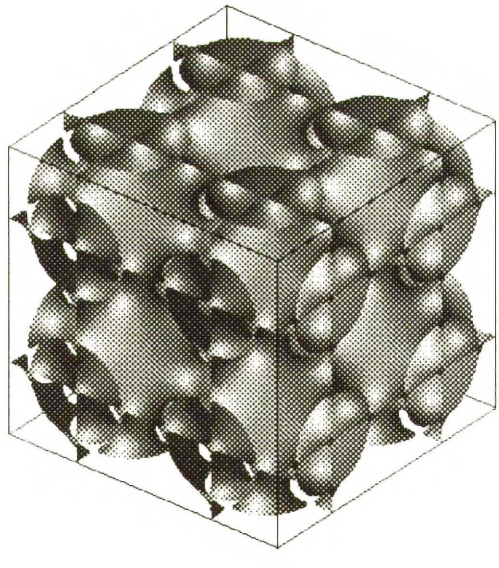

Figure 4.49: CD surface generated from the functional (2.9). The unit cell. Off diagonal view.

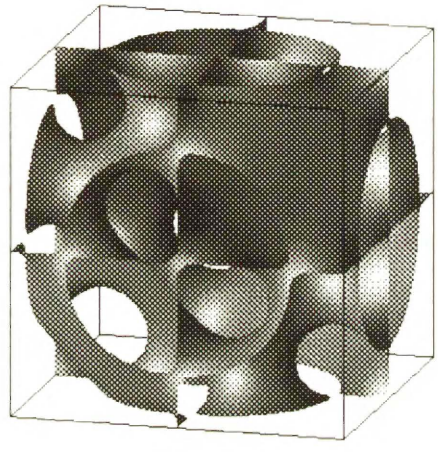

Figure 4.50: CD surface generated from the functional (2.9). 1/8 of the unit cell. Off front view.

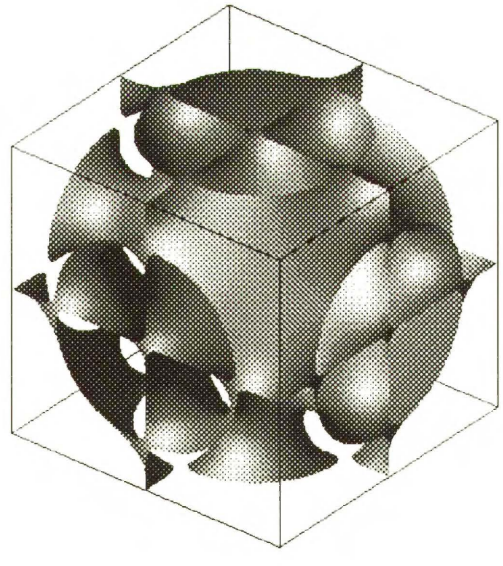

Figure 4.51: CD surface generated from the functional (2.9). 1/8 of the unit cell. Off diagonal view.

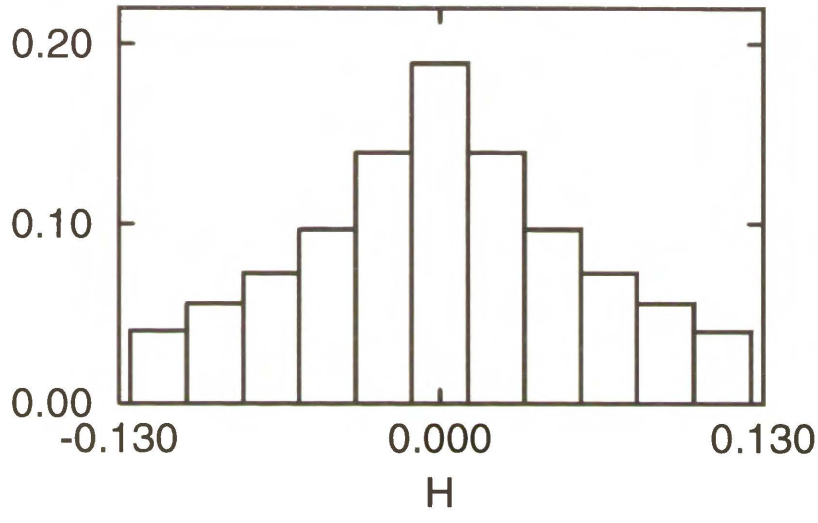

Figure 4.52: The histogram of the mean curvature for the surface CD

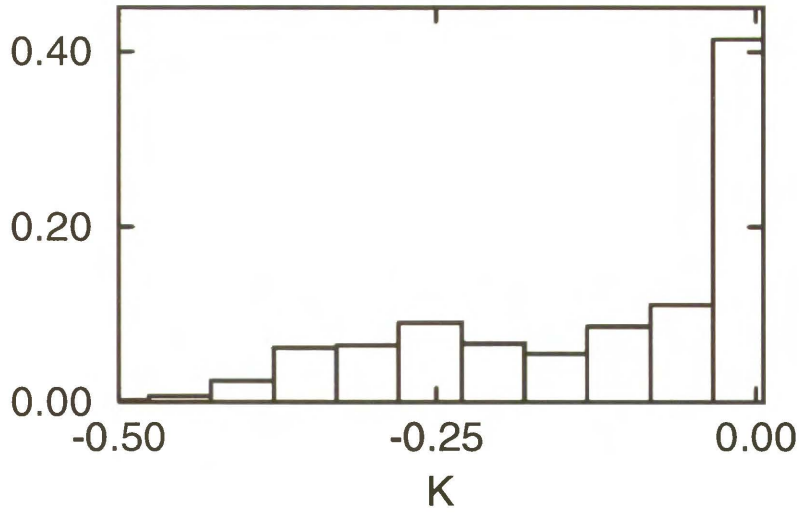

Figure 4.53: The histogram of the Gaussian curvature for the surface CD

The SCN1 surface is similar to BFY surface, but because its unit cell length is larger the surface is more complex. Comparison of these surfaces can be used as an example how the functional (2.9) keeps the size of water and oil region the same for different structures. For the bigger cell length the surface dividing the oil and water region is folded few times in order to keep the sizes of the oil and water region resulted from the functional (2.9) for a given values of the parameters f_0, g_0. It is amazing that the surface, representing the layer of surfactant in the model (2.9), is folded in such a way that its mean curvature tends to be zero.

The wealth of the high genus structures, even for the same symmetry, suggest the possibility of coexistence of these structures. We can speculate on the structure of microemulsion on the basis of these results. One can imagine that microemulsion is locally ordered like the phases we describe. Thus it is structured but globally disordered.

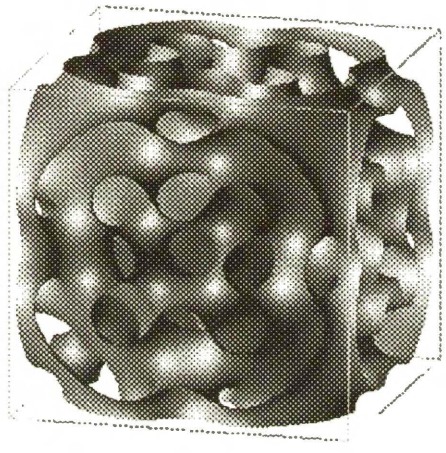

Figure 4.54: SCN1 surface generated from the functional (2.9). The unit cell. Off front view.

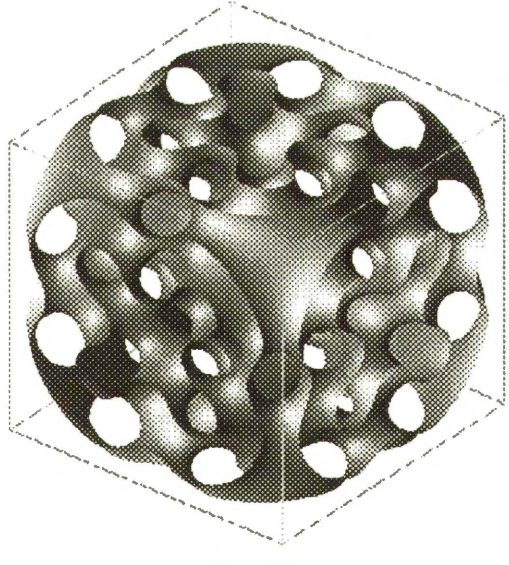

Figure 4.55: SCN1 surface generated from the functional (2.9). The unit cell. Off diagonal view.

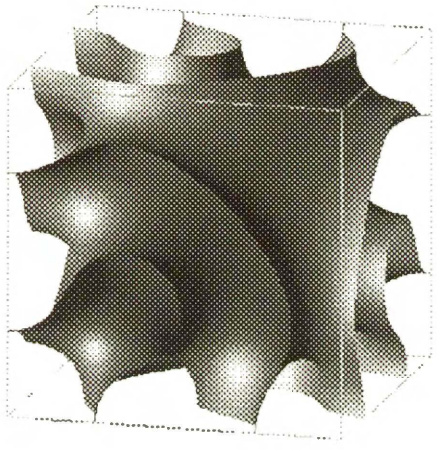

Figure 4.56: SCN1 surface generated from the functional (2.9). 1/8 of the unit cell. Off front view.

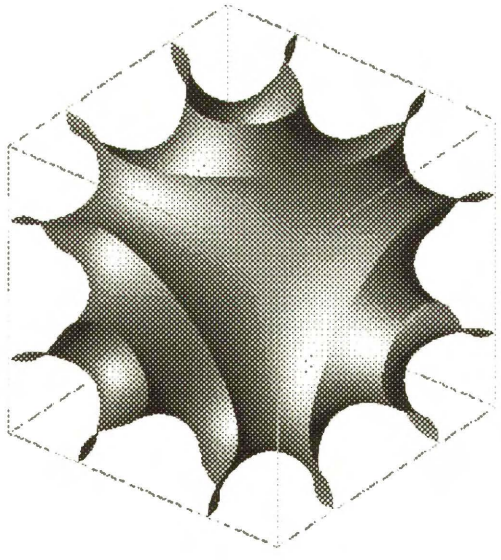

Figure 4.57: SCN1 surface generated from the functional (2.9). 1/8 of the unit cell. Off diagonal view.

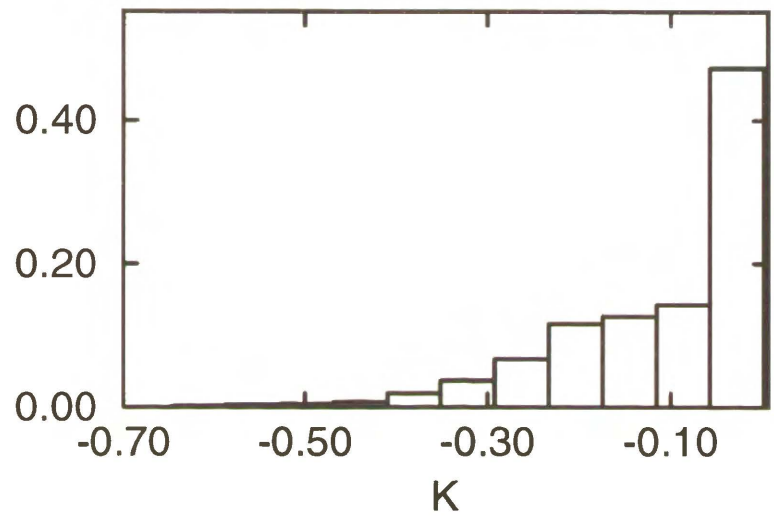

Figure 4.58: The histogram of the Gaussian curvature for the surface SCN1

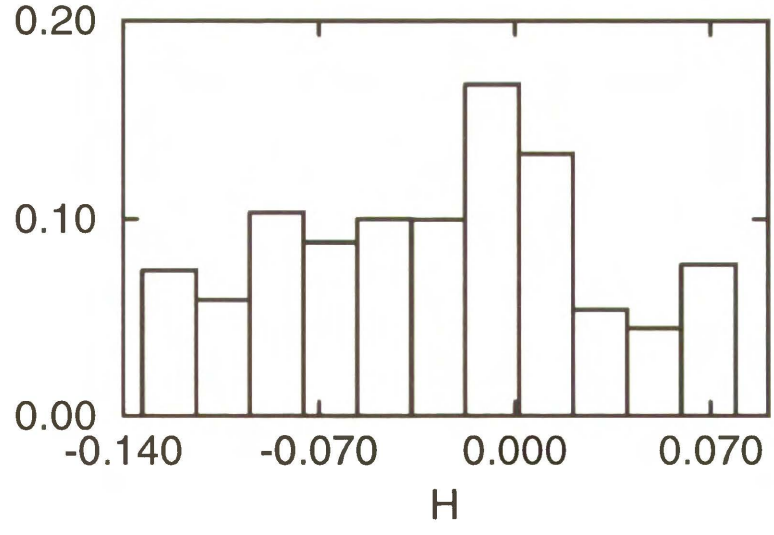

Figure 4.59: The histogram of the mean curvature for the surface SCN1

We have generated high genus surfaces of vanishing curvatures. The existence of such surfaces in real systems was questioned. The researches argued that it is impossible to build high genus periodic surface because of large curvatures, which could not be accommodated by the displacement of surfactant molecules at the surface [59]. As we can see from Table 4.3 high genus surfaces have large sizes of the unit cell and therefore their curvatures (see Gaussian curvatures) are similar in magnitude to those of surfaces of low genus. Therefore the argument against the existence of these surfaces does not hold.

The pictures of the high genus structures, especially the gyroid ones, strongly resemble the pictures of microemulsion taken during freeze fracture microscopy studies [5, 8]. The gyroid high genus surfaces have in general lower free energy that the surfaces of other symmetries. We can speculate that this symmetry would be preferred in real systems. In fact the Schoen gyroid G minimal surface is the most common in nature among the known minimal surfaces. The gyroid surfaces do not have planes of symmetry. This may cause easier adaptation of their shape to the structures encountered in nature, like diblock copolymers, lipid-water solution or surfactant mixtures.

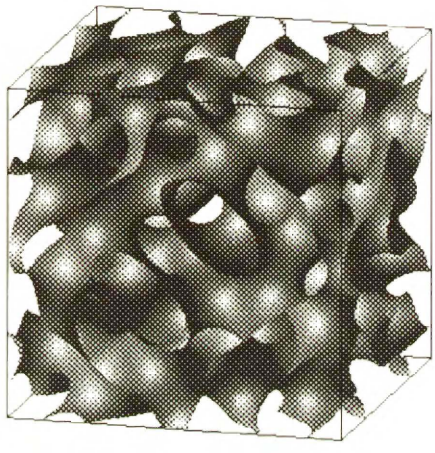

Figure 4.60: GX1 surface. The unit cell. Off front view.

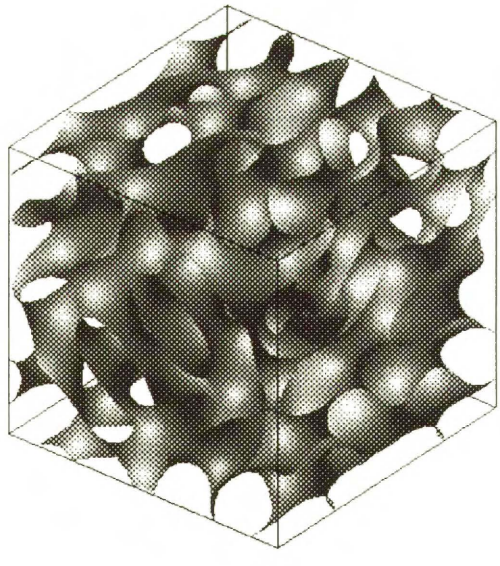

Figure 4.61: GX1 surface. The unit cell. Off diagonal view.

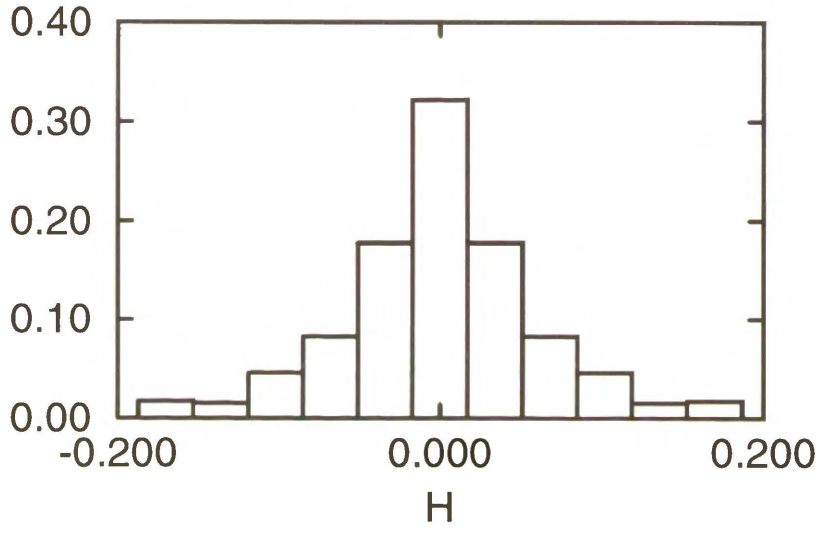

Figure 4.62: The histogram of the mean curvature for the surface GX1

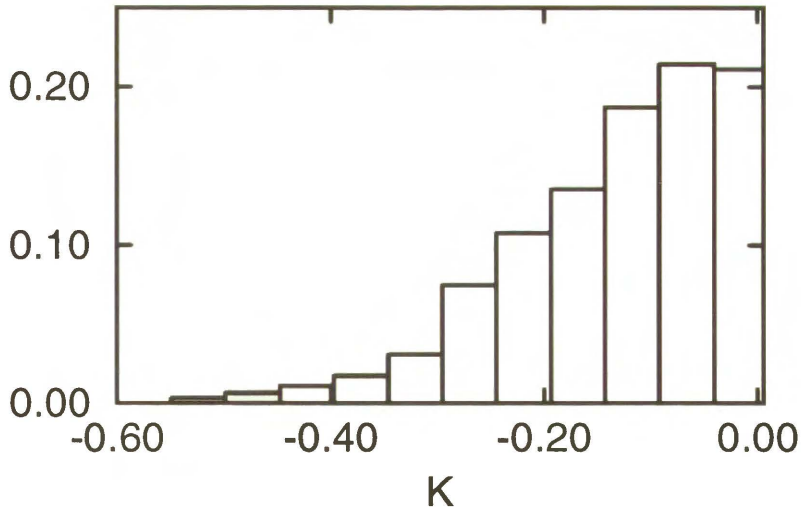

Figure 4.63: The histogram of the Gaussian curvature for the surface GX1

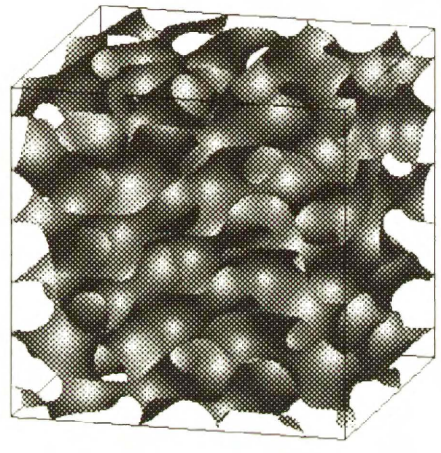

Figure 4.64: GX2 surface. The unit cell. Off front view.

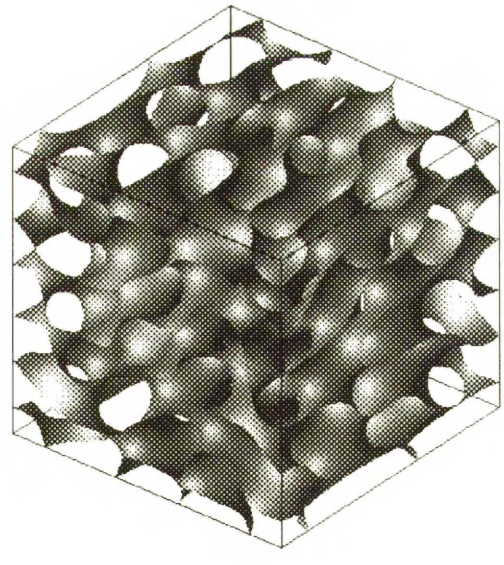

Figure 4.65: GX2 surface. The unit cell. Off diagonal view.

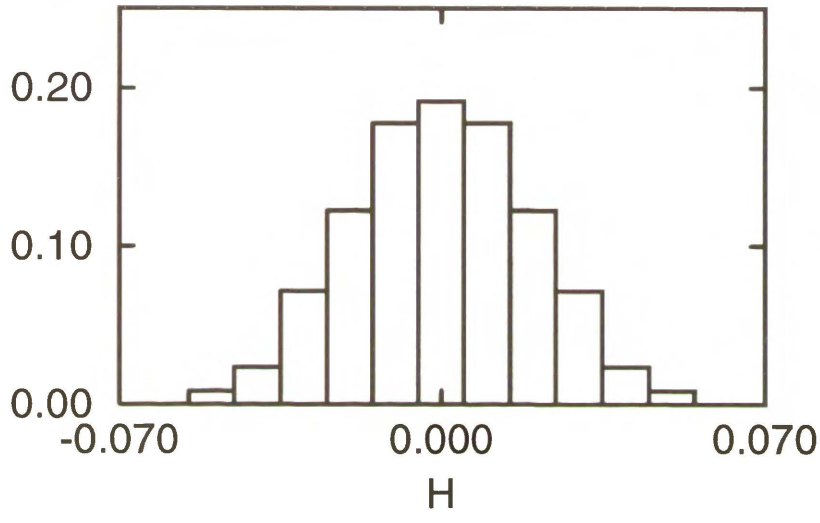

Figure 4.66: The histogram of the mean curvature for the surface GX2

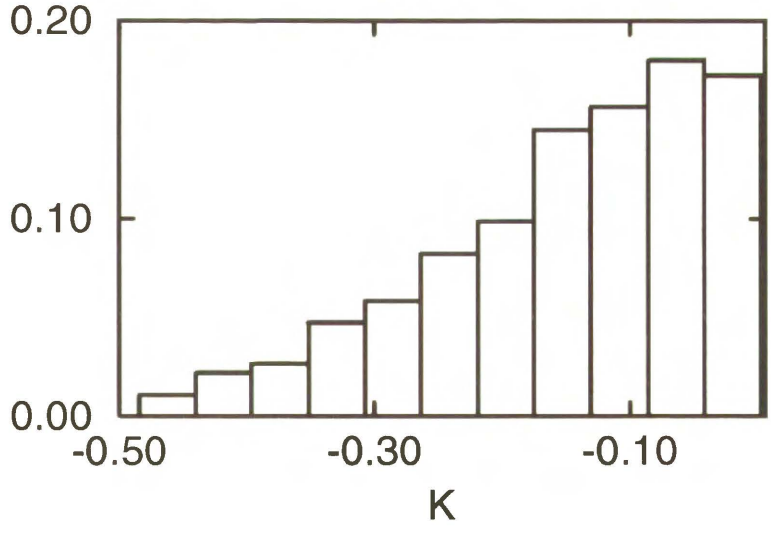

Figure 4.67: The histogram of the Gaussian curvature for the surface GX2

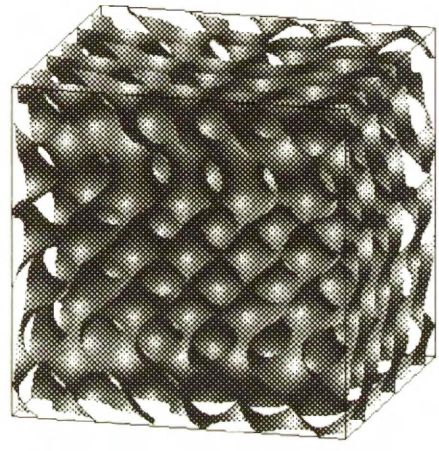

Figure 4.68: GX3 surface. The unit cell. Off front view.

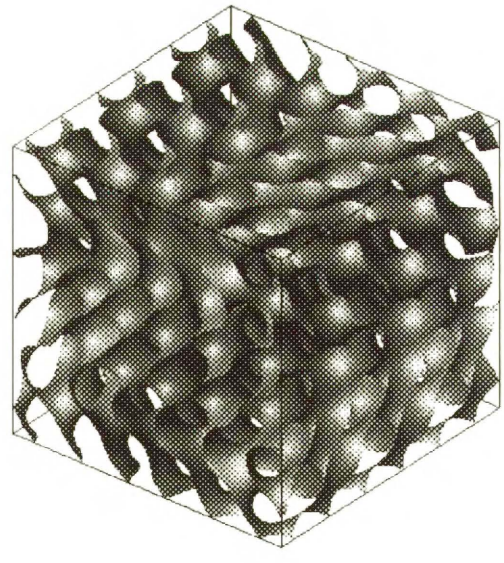

Figure 4.69: GX3 surface. The unit cell. Off diagonal view.

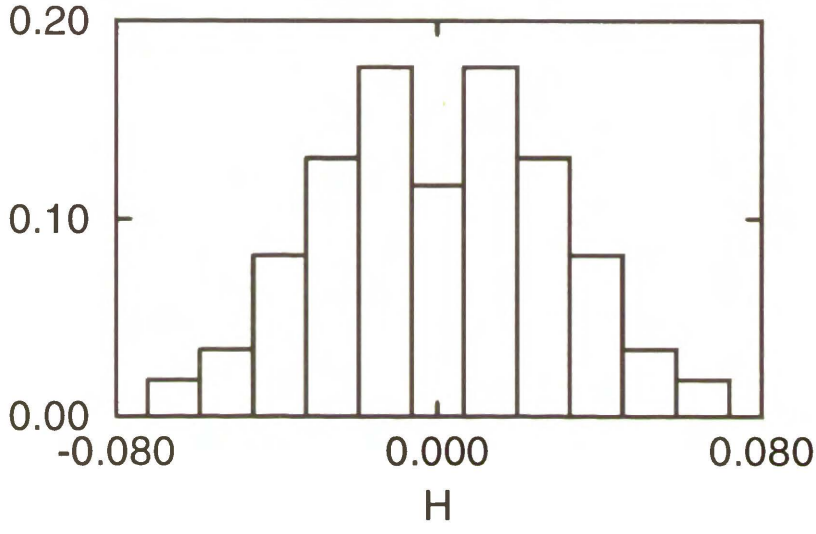

Figure 4.70: The histogram of the mean curvature for the surface GX3

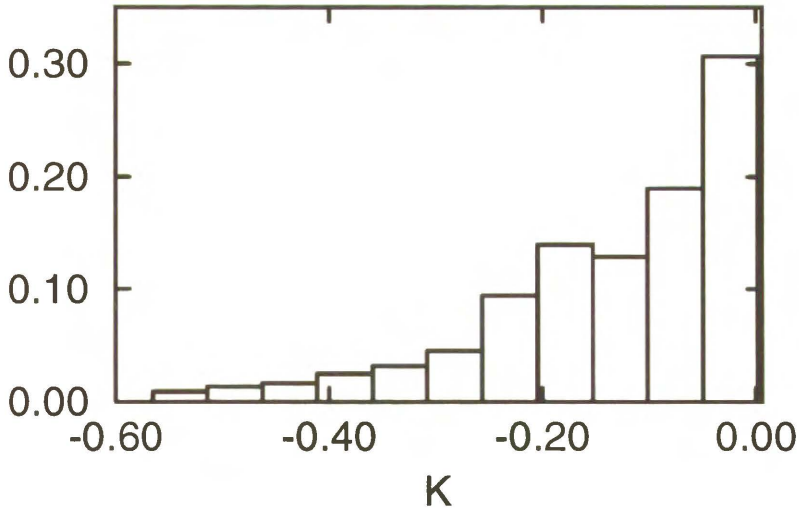

Figure 4.71: The histogram of the Gaussian curvature for the surface GX3

The properties of high genus surfaces are calculated with lower accuracy than the properties of those of low genus ones. It is so because we have used the same size of the lattice, N, for the unit cell. This results in bigger lattice spacing, h. For high genus structures more surface has to be accommodated in the unit cell, therefore the calculation of the derivatives is less accurate.

The biggest errors are in calculations of the curvatures, because all possible approximations are accommodated in these calculations. First is the approximation used to find the surface $\phi(\mathbf{r}) = 0$. The location of this surface has to be linearly interpolated between the lattice sites. The folmulas for the mean and Gaussian curvature are also numerical approximations of the analytic expressions. The derivatives used in calculations are also numerical approximations. The points used to calculate the derivatives have to be interpolated between the lattice sites. Finally the discretization and minimization of the functional also introduces some errors. It is amazing that, in spite of all those sources of errors, the curvatures are calculated with such a high accuracy, which can be seen looking at the histograms of the mean curvature for P,D,G minimal surfaces.

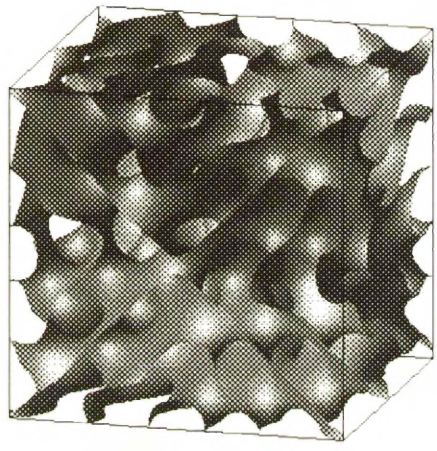

Figure 4.72: GX4 surface. The unit cell. Off front view.

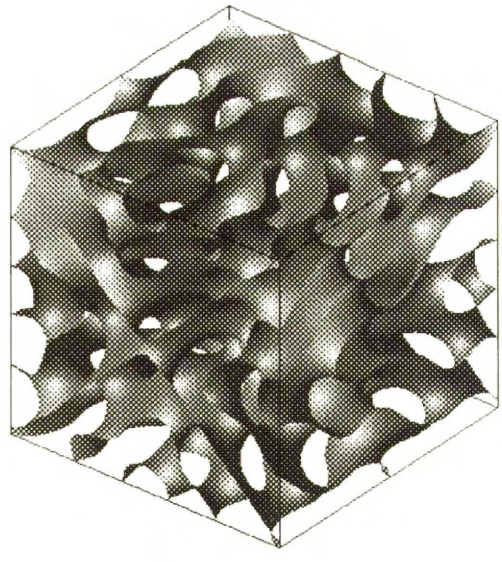

Figure 4.73: GX4 surface. The unit cell. Off diagonal view.

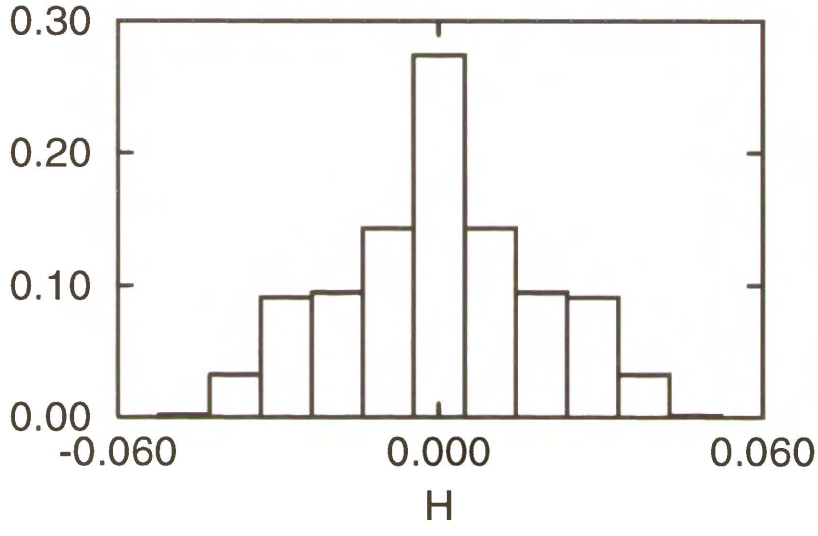

Figure 4.74: The histogram of the mean curvature for the surface GX4

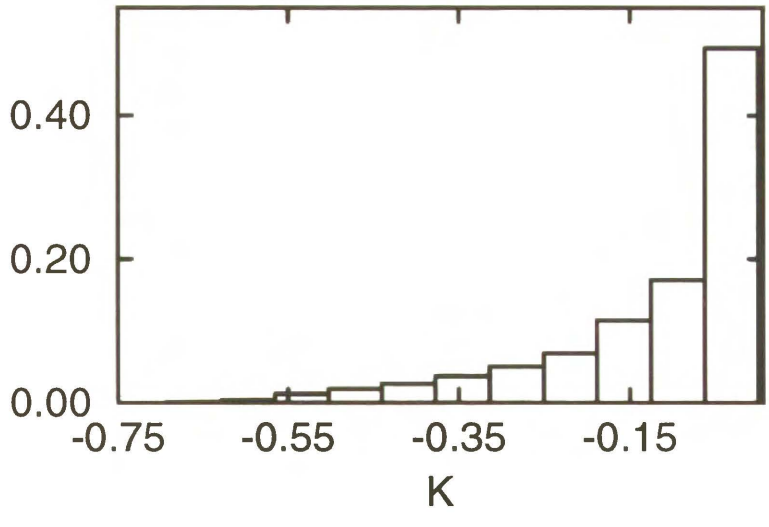

Figure 4.75: The histogram of the Gaussian curvature for the surface GX4

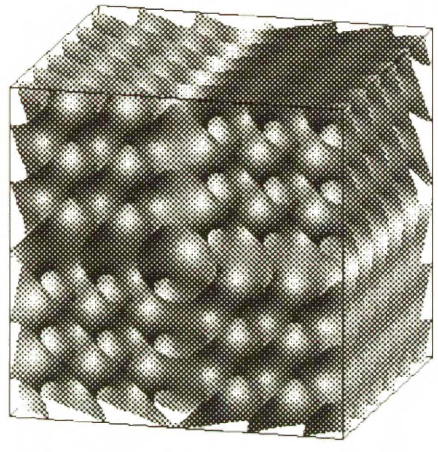

Figure 4.76: GX5 surface. The unit cell. Off front view.

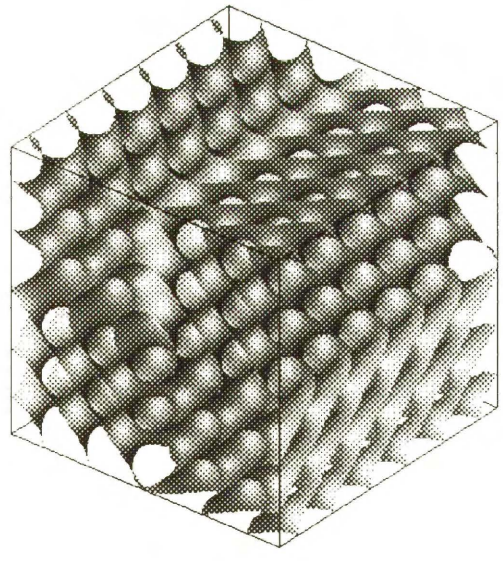

Figure 4.77: GX5 surface. The unit cell. Off diagonal view.

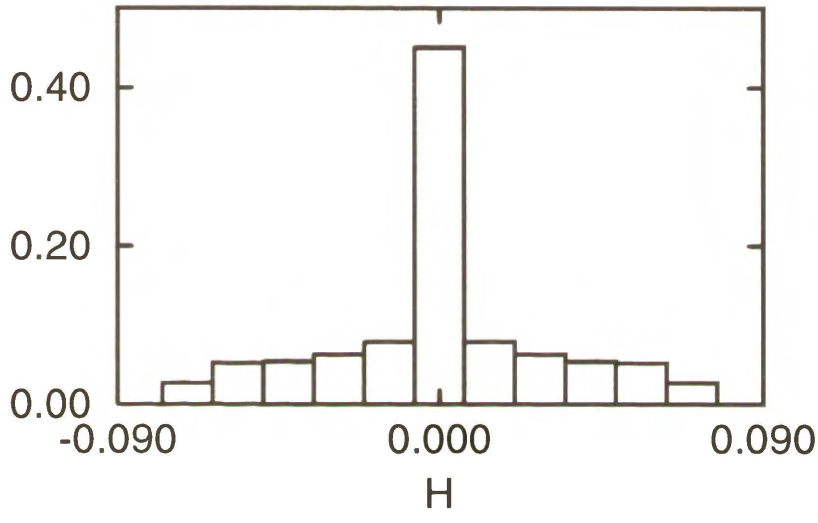

Figure 4.78: The histogram of the mean curvature for the surface GX5

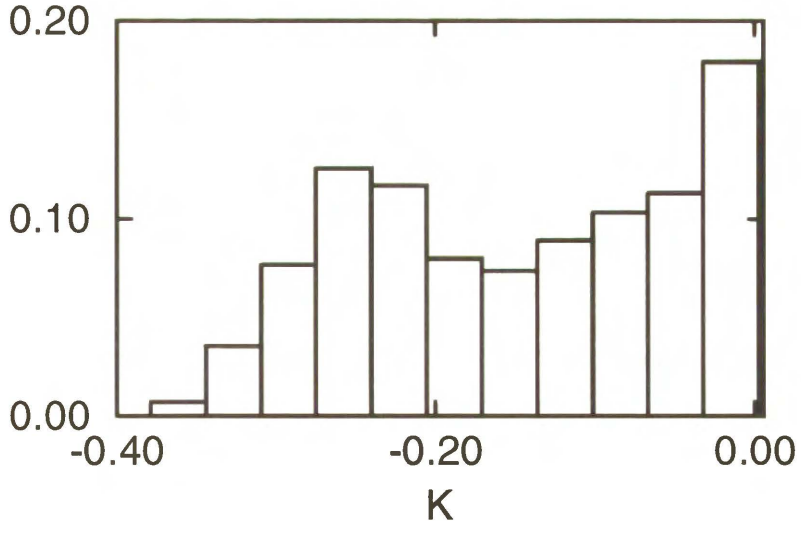

Figure 4.79: The histogram of the Gaussian curvature for the surface GX5

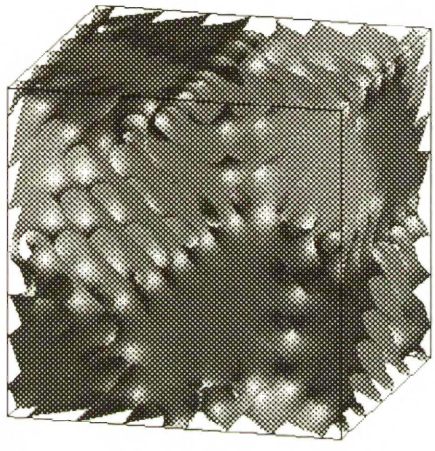

Figure 4.80: GX6 surface. The unit cell. Off front view.

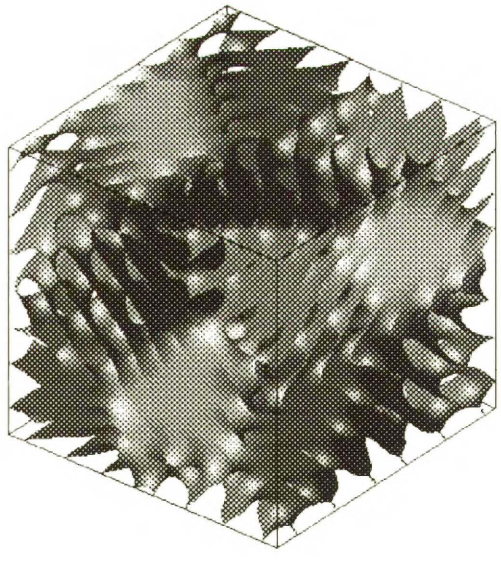

Figure 4.81: GX6 surface. The unit cell. Off diagonal view.

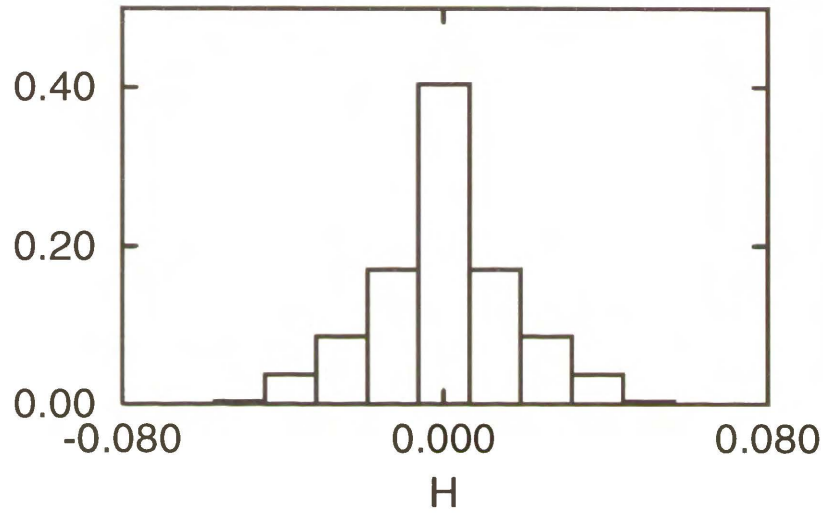

Figure 4.82: The histogram of the mean curvature for the surface GX6

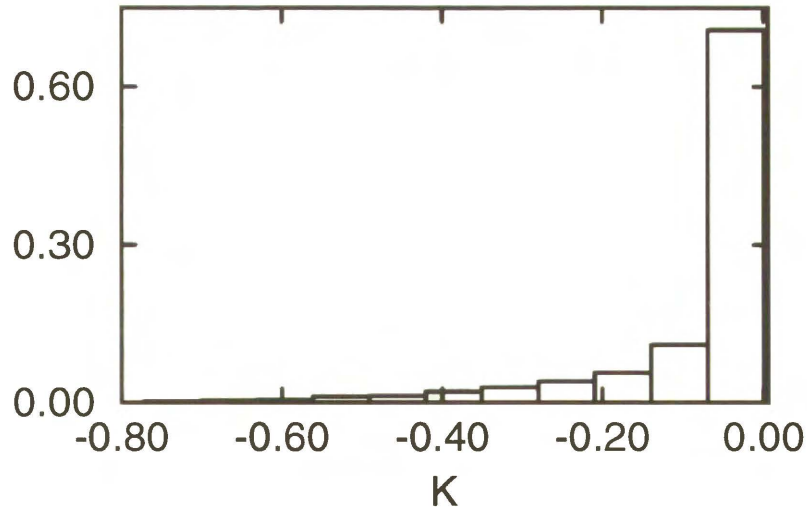

Figure 4.83: The histogram of the Gaussian curvature for the surface GX6

Name	Cell Length	Energy	Surface Area	Genus
SCN1	25.6	-0.178	7.4288	45
CD	28.88	-0.167	8.2257	73
GX1	25.36	-0.182	7.622	53
GX2	26.48	-0.183	8.081	69
GX3	31.72	-0.181	9.657	109
GX4	26.16	-0.186	7.907	53
GX5	34.40	-0.178	10.519	157
GX6	41.32	-0.186	12.459	141

Table 4.3: The geometrical properties of high genus surfaces obtained from the functional (2.9), for the parameters $f_0 = 0.0$, $g_0 = -3.0$. Surface area $\tilde{S}$, in the table, is the normalized per face of the unit cube L^2 surface area S of the interface in the unit cell, $\tilde{S} = S/L^2$, $L = (N-1)h$. The energy is given per unit volume. The volume fraction for all structures is 0.5.

4.4 Multiply continuous embedded periodic surfaces

The possibility of the existence of multiply continuous structures was never discussed so far to the best of our knowledge. Although the idea seems to be trivial nobody has considered it. So far only bicontinuous phases have been considered both in the theoretical and experimental studies. In the bicontinuous structure the single surface separates the volume into two disjoint subvolumes. In our phases there is more than one periodic surface which disconnects the volume into three or more disjoint subvolumes.The experimental results do not rule out the existence of such structures, contrary the experiment on the electrical conductivity support the idea [5, 6]. It would be very interesting to design an experiment answering the question whether the structures considered so far as bicontinuous are only bicontinuous or maybe they are multiply continuous.

The multiply continuous structures are most easily generated for the values of parameters f_0 and g_0 in (2.9) taken near the boundary of lamellar and water (oil) phase and for the bigger unit cell length, $L = (N-1)h$, than the length of structures of low genus.

We present the multiply continuous structures of the simple cubic phase symmetry (SCL1,SCL2, Figs. 4.84,4.86) and of the gyroid phase symmetry (GL1,GL2 Figs. 4.88,4.90). The SCL1 structure is triply continuous, the GL1,SCL2 are four-tuply continuous, and GL2 is six-tuply continuous. For bigger size of the unit cell one is able to generate the structures n-tuply

continuous. It is remarkable that the volume fraction of oil and water is 0.5 for all these structures. The genera for all surfaces in a given structure are the same. Other properties of the multiply continuous structures are described in Table 4.4.

The SCL1 surface is especially interesting. Although the outer and inner surface looks different, see Fig. 4.84, they have the same surface area, see Table 4.4. In fact they are built of the same piece of the surface. The picture of 1/8 of the unit cell, see Fig. 4.85, explains how two different periodic surfaces can be built of the same surface patch.

The SCL2 structure is composed of three different embedded periodic surfaces, Figs. 4.86,4.87. The middle surface is the Schwarz minimal surface P, its normalized surface area of these surfaces are the same within the numerical errors, see Tables 4.4, 4.1. Similar, the middle phase surface in GL1 structure is the Schoen minimal surface G.

The GL2 structure suggest that one can generate arbitrary n-tuply continuous structures. It is only necessary to set the cell length sufficiently large. We have not attempted generation of such structures because, due to the limits imposed by computer memory and speed of processor, the lattice spacing would be too big for a given size of the lattice to obtain reasonable accuracy.

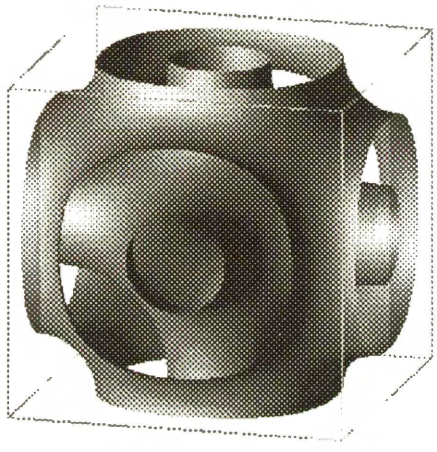

Figure 4.84: SCL1 surface generated from the functional (2.9). The unit cell. Off front view.

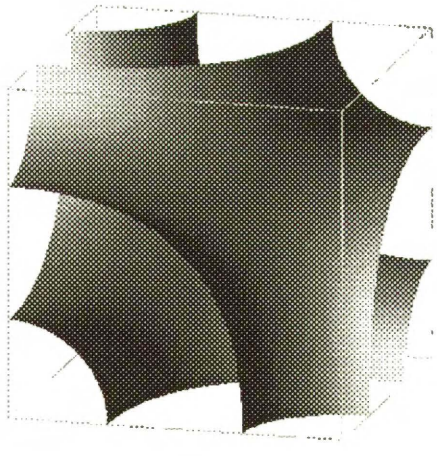

Figure 4.85: SCL1 surface generated from the functional (2.9). 1/8 of the unit cell. Off front view.

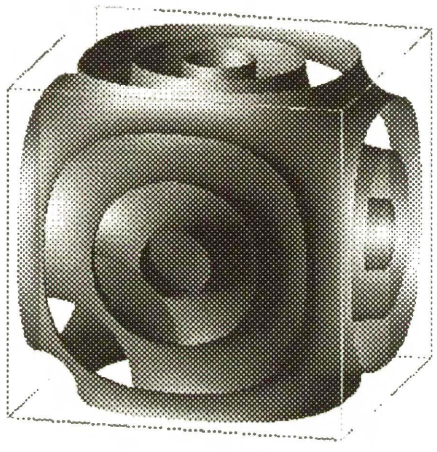

Figure 4.86: SCL2 surface generated from the functional (2.9). The unit cell. Off front view.

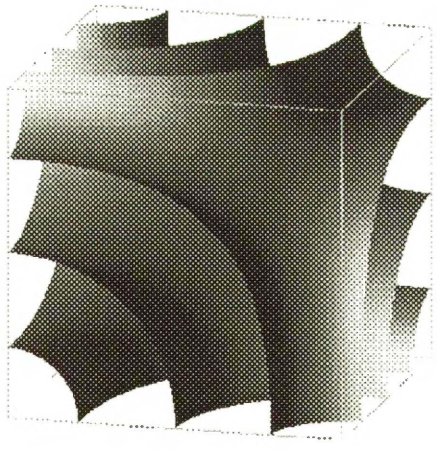

Figure 4.87: SCL2 surface generated from the functional (2.9). 1/8 of the unit cell. Off front view.

Figure 4.88: GL1 surface generated from the functional (2.9). The unit cell. Off front view.

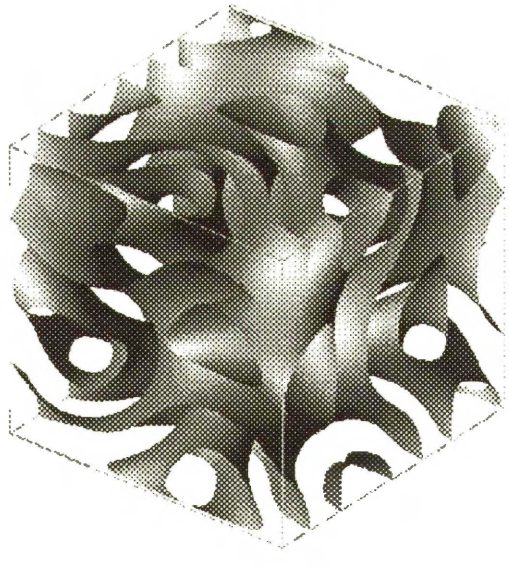

Figure 4.89: GL1 surface generated from the functional (2.9). The unit cell. Off diagonal view.

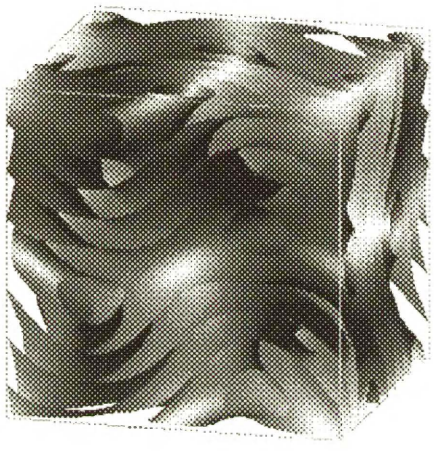

Figure 4.90: GL2 surface generated from the functional (2.9). The unit cell. Off front view.

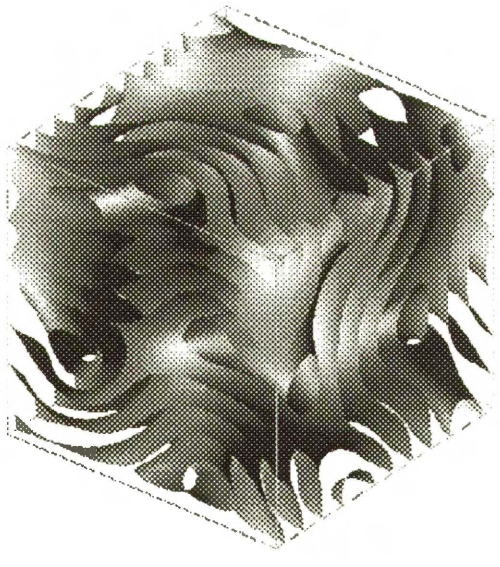

Figure 4.91: GL2 surface generated from the functional (2.9). The diagonal cell. Off front view.

Name	Cell Length	Energy	Surface Area	Genus
SCL1	14.96	-0.175	4.090	3
1			2.045	
2			2.045	
SCL2	21.14	-0.178	5.780	3
1			1.716	
2			2.348	
3			1.716	
GL1	26.32	-0.187	7.546	5
1			2.226	
2			3.096	
3			2.226	
GL2	41.16	-0.185	11.887	5
1			1.659	
2			2.736	
3			3.097	
4			2.736	
5			1.659	

Table 4.4: The geometrical properties of multiply continuous structures obtained from the functional (2.9), for the parameters $f_0 = 0.0$, $g_0 = -3.0$. Surface area $\tilde{S}$, in the table, is the normalized per face of the unit cube L^2 surface area S of the interface in the unit cell, $\tilde{S} = S/L^2$, $L = (N-1)h$. The energy is given per unit volume. The volume fraction for all surfaces is 0.5. The genus is given for any single surface in the structure.

4.5 Stability of different phases in the model

We have investigated many bicontinuous phases of different symmetries, genera and dimensions of the unit cell. The bicontinuous phase with the lowest value of the free energy turned out to be the gyroid, but the only stable liquid crystalline phase in this model is the lamellar phase. Fig. 4.92 shows the plot of the free energy as the function of the parameter f_0 for the lamellar and gyroid phase. The phase diagram for the model (2.9), in mean-field

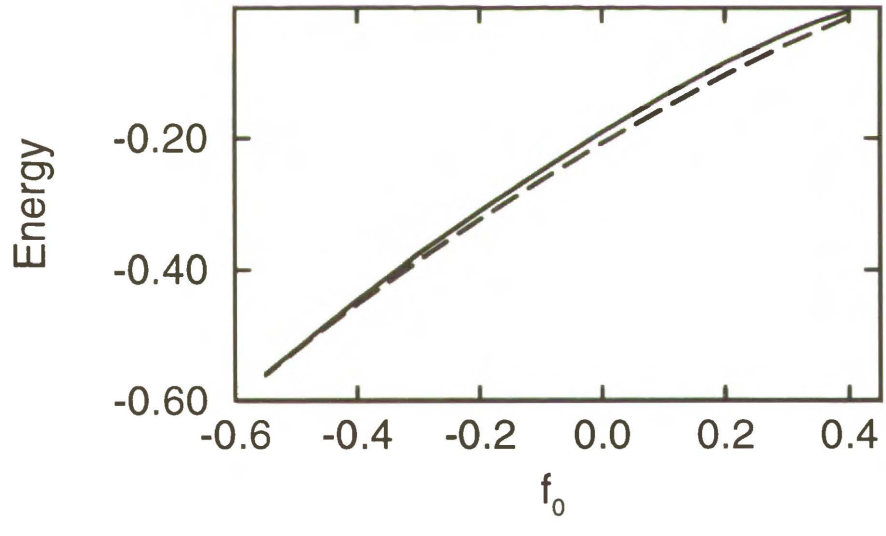

Figure 4.92: The free energy per unit volume for the lamellar phase (dashed line) and gyroid phase (solid line) for the model (2.9). The parameter g_0 was equal to -3.0.

approximation, calculated by Gompper and Zschocke [21] and checked here is shown in Fig. 4.93. Other bicontinuous phases behave in the same way

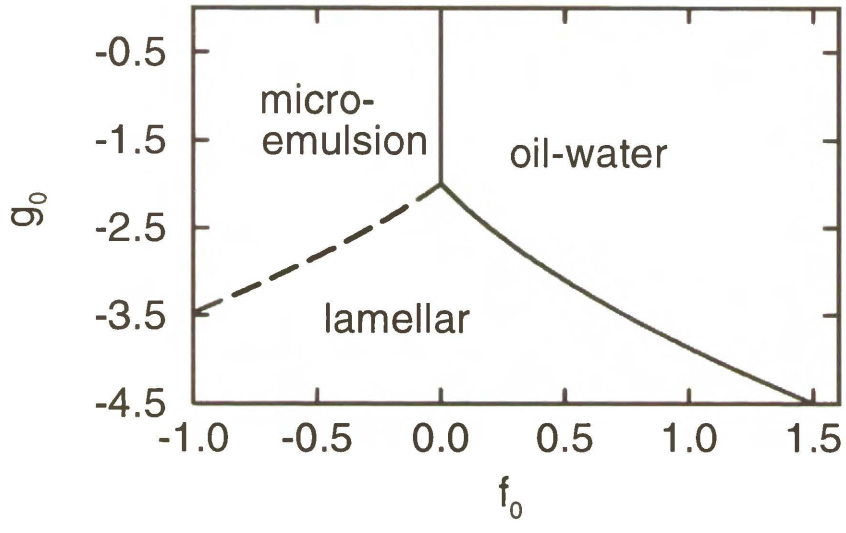

Figure 4.93: The phase diagram for the model (2.9)

as the gyroid and lamellar. The value of the free energy in the vicinity of microemulsion boundary converges to the value of the free energy for the microemulsion.

We have also studied the stability of bicontinuous phases for different function describing surfactant, $g[\phi(\mathbf{r})]$. We have used the following form of $g[\phi(\mathbf{r})]$:

$$g\big[\phi(\mathbf{r})\big] = g_2\phi(\mathbf{r})^4 + g_0. \tag{4.4}$$

We have expected that this form of $g[\phi(\mathbf{r})]$ would make the interface between oil and water sharper and therefore it would lower the free energy. The in-

terface indeed was sharper as we expected, but the unit cell length decreased also. This resulted in higher values of the free energy than before and all bicontinuous phases were metastable as in the previous case. It might suggest that one order parameter functional is not sufficient to describe the behavior of ordered phases. Howver, it has been observed recently [60] that one may expect the stabilization of the gyroid phase in Monte Carlo simulation. Thus the fluctuations can play a significant role in the stabilization of bicontinuous phases. We note that in the case of multi-parameter Landau models introduced in recent years [5] we may expect the stabilization of the various phases which in the one order parameter Landau model are only metastable [25]. Our current results are a very good starting point for investigation of the stability of bicontinuous phases in multi-parameter Landau functionals.

Chapter 5

Summary and Conclusion

The method of solving the functional (2.9), we have applied, allowed us to make several discoveries. **We have discovered that the solutions of the physical model of microemulsion can be triply periodic minimal surfaces**. To the best of our knowledge this is the first such discovery. So far the triply periodic minimal surfaces were generated from the Weirstrass representation or from the definition of the mean curvature.

We have discovered many triply periodic surfaces of non-positive Gaussian curvature. Some of them may be new minimal surfaces. Especially interesting are the surfaces of high genus. The existence of such surfaces may suggest that microemulsion can be such a surface of very high genus. For over one hundred years mathematicians have discovered a few infinite embedded periodic minimal surfaces of cubic symmetry. **We have discovered**, by using our method, **several new infinite periodic surfaces of cubic symmetry**, which are very likly to be miminal. The problem of peridic

surfaces is being rediscovered over recent years because of their importance in physich and biology. We are convinced that this work will help to make other workers signifacant progress in this area.

We have discovered, never considered yet, multiply continuous cubic structures formed in ternary mixtures of water, oil and surfactant. The idea of multiple continuity of cubic structures is the novel one. Our results call for new experimental techniques which could be used to discern between bicontinuous and multiply continuous structures. We hope that these new structures will soon be discovered in real systems.

Very often to see means to understand. We have not only calculated the properties of many cubic structures, investigated their stability, but also presented the pictures of new structures. We hope that this will help other workers better understand the phenomena in ternary liquid mixtures, diblock copolymers, and biological systems.

We have presented the general method for the generation of periodic surfaces of non-positive Gaussian curvature. This method can be well applied by physicists working in soft condensed matter, mathematicians working in topology, biologists and crystallographers. We are positive that the richness of the method is far from being explored by our work.

The answers we have given in this work do not close the problem we have investigated. Contrary, our results open new area to investigate by other workers, can be a pointer for experimentalists to design new experiments. Our results are also an ideal starting point, for theoreticians, to pursue the studies of Landau-Ginzburg models with more than one order parameter

field [25], to investigate dynamical properties of complex systems [61, 62] or to study complex fluids in confined geometries [22]. These are only a few benefits of this work and we are convinced that this is not a complete list.

Bibliography

[1] R. G. Laughlin, *The aqueous phase behavior of surfactants*, Academic Press, London, 1994.

[2] V. Degiorgio and M. Corti, editors, *Physics of Amphiphiles: Micelles, Vesicles and Microemulsions*, Amsterdam, The Netherlands, 1985, Italian Physiscal Society, North-Holland Physics Publishing.

[3] M. Kalhweit et al., J. Colloid Interface Sci. **118**, 436 (1987).

[4] M. Kahlweit et al., Langmuir **4**, 499 (1988).

[5] G. Gommper and M. Schick, *Self-Assembling Amphiphilic Systems*, volume 16 of *Phase Transitions and Critical Phenomena*, Academic Press, first edition, 1994.

[6] A. Ciach, Pol. J. Chem. **66**, 1347 (1992).

[7] K. V. Schubert and R. Strey, J. Chem. Phys. **95**, 8532 (1991).

[8] W. Jahn and R. Strey, J. Phys. Chem. **92**, 2294 (1988).

[9] A. Ciach and A. Poniewierski, Phys. Rev. E **52**, 596 (1995).

[10] H. Chung and M. Caffrey, Nature **368**, 224 (1994).

[11] Z. Gang Wang and S. A. Safran, Europhys. Lett. **11**, 425 (1990).

[12] R. Lipowsky, Nature **349**, 475 (1991).

[13] W. Helfrich, Z. Naturforsch A **28**, 693 (1973).

[14] L. D. Landau and E. M. Lifshitz, *Statistical Physics*, Pergamon Press, 3 edition, 1989.

[15] M. Teubner and R. Strey, J. Chem. Phys. **87**, 3195 (1987).

[16] G. Gompper and M. Schick, Phys. Rev. Lett. **65**, 1116 (1990).

[17] G. Gompper, R. Hołyst, and M. Schick, Phys. Rev. A **43**, 3157 (1991).

[18] J. Putz, R. Hołyst, and M. Schick, Phys. Rev. A **46**, 3369 (1992).

[19] G. Gompper and M. Hennes, J. Chem. Phys. **102**, 2871 (1994).

[20] G. Gompper and S. Zschocke, Europhys. Lett. **16**, 731 (1991).

[21] G. Gompper and S. Zschocke, Phys. Rev. A **46**, 4836 (1992).

[22] F. Schmid, Phys. Rev. E **48**, 1882 (1993).

[23] G. Gompper and J. Goos, Phys. Rev. E **50**, 1325 (1994).

[24] M. Laradji, H. Guo, M. Grant, and M. J. Zuckermann, Phys. Rev. A **44**, 8184 (1991).

[25] A. Ciach, J. Chem. Phys. **104**, 1 (1996).

[26] K. Kawasaki and T. Kawakatsu, Physica A **164**, 549 (1990).

[27] G. Gompper and S. Klein, J. Phys. II France **2**, 1725 (1992).

[28] G. Gompper and M. Kraus, Phys. Rev. E **47**, 4301 (1993).

[29] W. Góźdź and R. Hołyst, Macromol. Theory Simul. in press (1996).

[30] M. Abramowitz and I. A. Stegun, editors, *Handbook of Mathematical Functions With Formulas, Graphs, and Mathematical Tables*, volume 55 of *National Bureau of Standards Applied Mathematics Series*, U. S. Government Printing Office, Washington, D.C. 20402, 9th edition, 1970, pages 883-884.

[31] D. A. Hoffman, J. de Physique Colloque **51 C7**, 197 (1990).

[32] D. M. Anderson, H. T. Davis, L. E. Scriven, and J. C. C. Nitsche, Adv. Chem. Phys. **77**, 337 (1990).

[33] S. T. Hyde, Z. Kristallogr. **187**, 165 (1989).

[34] I. S. Barnes, S. T. Hyde, and B. W. Ninham, J. de Physique Colloque **51 C7**, 19 (1990).

[35] A. L. Mackay and J. Klimowski, Comp. and Maths. with Appls. **12B**, 803 (1986).

[36] M. Spivak, *A Comprehensive Introduction to Differential Geometry*, volume III, Publish or Perish, Berkley, 1979.

[37] H. Coxeter, *Regular Polytopes*, MacMillan, New York, 1963.

[38] N. S. M. Henry and K. Lonsdale, editors, *International Tables for X-ray Crystallography*, volume 1, The Kynoch Press, Birmingham, England, 1952.

[39] A. H. Schoen, Inifinite periodic minimal surfaces without self-intersections, Technical Report TN D-5541, NASA, 1970.

[40] W. H. Press, B. P. Flannery, S. A. Teukolsky, and W. T. Vetterling, *Numerical Recipes*, Cambridge University Press, 1990.

[41] J. A. F. Plateau, *Statique Expérimentale et Théorique des Liquides aux Seules Forces Moléculaires*, volume 2, Gauthier-Villars, Trubner et Cie, F. Clemm, 1873.

[42] L. E. Scriven, Nature **263**, 123 (1976).

[43] V. Luzzati and P. A. Spegt, Nature **215**, 701 (1967).

[44] V. Luzzati, A. Tardieu, and T. Gulik-Krzywicki, Nature **217**, 1028 (1968).

[45] V. Luzzati, T. Gulik-Krzywicki, and A. Tardieu, Nature **218**, 1031 (1968).

[46] V. Luzzati, A. Tardieu, T. Gulik-Krzywicki, E. Rivas, and F. Reiss-Husson, Nature **220**, 485 (1968).

[47] E. L. Thomas, D. M. Anderson, C. Henkee, and D. Hofman, Nature **334**, 598 (1988).

[48] A. L. Mackay, Nature **314**, 604 (1985).

[49] H. G. von Schnering and R. Nesper, Angewandte Chemie, International Edition in English **26**, 1059 (1987).

[50] H. Terrones, J. de Physique Colloque **51 C7**, 345 (1990).

[51] S. Lidin, S. T. Hyde, and B. W. Ninham, J. Phys. France **51**, 801 (1990).

[52] A. Fodgen, J. de Physique Colloque **51 C7**, 149 (1990).

[53] E. L. Thomas, D. B. Alward, D. J. Kinning, D. C. Martin, and L. J. Fetters, Macromolecules **19**, 2187 (1986).

[54] H. Hasegawa, H. Tanaka, K. Yamasaki, and T. Hashimoto, Macromolecules **20**, 1651 (1986).

[55] D. J. Kinning, J. M. Ottino, and E. Thomas, Macromolecules **20**, 1129 (1986).

[56] D. A. Hajduk et al., Macromolecules **27**, 4063 (1994).

[57] D. Cvijović and J. Klimowski, Chem. Phys. Lett. **226**, 93 (1994).

[58] D. M. Anderson, ., PhD thesis, University of Minesota, 1986.

[59] S. T. Hyde, J. Phys. Chem. **93**, 1458 (1989).

[60] R. Hołyst and W. Góźdź, The structure of microemulsion from Monte Carlo simulations, unpublished results, 1996.

[61] G. Gompper and M. Hennes, Europhys. Lett. **25**, 193 (1994).

[62] G. Gompper and M. Hennes, Phys. Rev. Lett. **73**, 1114 (1994).

[63] A. Ciach, J. S. Høye, and G. Stell, J. Phys. A **21**, L777 (1988).

[64] A. Ciach, J. S. Høye, and G. Stell, J. Chem. Phys. **90**, 1214 (1989).

[65] A. Ciach, J. S. Høye, and G. Stell, J. Chem. Phys. **90**, 1222 (1989).

[66] A. Ciach, J. Chem. Phys. **96**, 1399 (1992).

[67] G. Gompper and M. Kraus, Phys. Rev. E **47**, 4289 (1993).

[68] G. Gompper and M. Schick, Phys. Rev. E **49**, 1478 (1994).

[69] W. Góźdź and R. Hołyst, Phys. Rev. Lett. , submitted (1996).

[70] W. Góźdź and R. Hołyst, Phys. Rev. Lett. , submitted (1996).

[71] S. Lidin, J. de Physique Colloque **51 C7**, 237 (1990).

Streszczenie pracy doktorskiej

"Statystyczna teoria mieszanin zawierających surfaktanty"

We wstępie opisane zostały podstawowe własności mieszanin zawierających surfaktant. Celem pracy bylo zbadanie mezoskopowej struktury takich mieszanin, a w szczególności powierzchni tworzonych przez cząsteczki surfaktantu na granicy faz wody i oleju

W rozdziale drugim opisano model funkcjonału Landaua-Ginzburga zaproponowany do opisu powierzchni w badanych mieszaninach. Użyty zostal funkcjonal Landaua-Ginzburga z jednym skalarnym parametrem uporządkowania reprezentującym różnicę koncentracji wody i oleju.

W rozdziale trzecim zostałopisany sposób rozwiazania funkcjonału Landaua-Ginzburga oraz sposób obliczania wielkości charakteryzujących powierzchnie tworzone przez cząsteczki surfaktantu.

W rozdziale piątym przedstawiono otrzymane wyniki. Został zaproponowany nowy sposób genrowania powierzchni o ujemnej krzywiźnie Gaussowskiej. Zostalo odkryte, że rozwiazaniami modelu Landaua-Ginzburga opisujacego mieszaniny zawierajace surfaktant są trójperiodyczne powierzchnie minimalne. Zostało odkryte kilkanaście nowych rodzajów trójperiodycznych powierzchni o ujemnej krzywiźnie Gaussowskiej. Wiele z tych powierzchni jest najprawdopodobniej powierzchniami minimalnymi. Odkryto nowe, nigdy do tej pory nie dyskutowane w literaturze struktury wielociągłe.